Computational Characterization of Decision Making During Trans-saccadic Visual Perception

Pierre G. Gianferrara[1*], Weiwei Zhou[1], Tyler A. Lesh[2], Timothy D. Hanks[3,4], Cyndi L. Edelman[2], Cameron S. Carter[3,5], Wilsaan M. Joiner[1,4]

[1]Department of Neurobiology, Physiology and Behavior, University of California, Davis, Davis CA 95616

[2]Department of Psychiatry, University of California, Davis, Davis CA 95616

[3]Center for Neuroscience, University of California, Davis, Davis CA 95616

[4]Department of Neurology, University of California, Davis, Davis CA 95616

[5]Department of Psychiatry & Human Behavior, University of California, Irvine, Irvine CA 92697

*Corresponding author: pgianfer@ucdavis.edu

Abstract

When sampling visual information from the environment, humans execute fast sequential saccadic eye movements and yet preserve stability in their visual percept. This ability relies on the continuous integration of external sensory information (e.g., visual displacements) and internal monitoring signals. At the time of the saccade subjects often experience saccadic suppression of displacement—a failure to notice changes in the location of visual objects slightly shifted during the eye movement. Although well studied, questions remain regarding *how* and *when* external sensory signals lead to perceptual judgment alterations following saccadic eye movements. Here we used a drift diffusion modeling (DDM) framework to systematically examine the extent to which sensory information biased perceptual judgments when detecting trans-saccadic shifts of visual targets. Healthy human participants (N = 30, 21 female) completed a visual perception task in which a visual target was shifted following a prompted saccadic eye movement (4° or 8°). Target displacements occurred up to $\pm 2.5^{o}$ along the horizontal axis, and participants reported the shift direction with a button press response. Incorporating the perceptual response and visual error between the displaced target and end-movement fixation location, the DDM accounted for the visuospatial biasing effects of sensory processing on decision-making. The modeling framework based on the visual error could also capture individual positive and negative biasing effects across backward shifts (i.e., towards the initial fixation location) and forward shifts (i.e., further away from initial fixation). Furthermore, participants whose perceptual bias was more pronounced in either the backward or forward directions tended to show a greater visuospatial offset in evidence accumulation preceding perceptual judgments due to an overreliance on the visual error information. The DDM computational modeling approach described here shows promise as an

explanatory framework to account for sensorimotor integration impairments based on perceptual deficits demonstrated in certain patient populations.

Author Summary

Maintaining a stable visual percept relies on the integration of externally-generated sensory signals from the environment and internally-generated predictive signals based on executed eye movements. Previous work has found that subjects often fail to detect object location changes in the scene at the time of rapid eye movements (saccades). In this work, we provide a computational framework (a modified drift diffusion model) to quantitatively establish the relative contribution of sensory error signals (i.e., the visual error) to perceptual judgments and decision-making behavior following saccades. We show that greater reliance on the visual error leads to increased biasing effects on response accuracy and manual reaction time. These effects are characterized by an offset in the drift rate, representing evidence accumulation, which predict lower accuracy in perceptual reports of trans-saccadic visual shifts. Collectively, the results provide new measures of visual error-based biases on decision-making, which could serve as behavioral markers for neurophysiological investigations of patient populations.

Introduction

One remarkable property of the visual system is its ability to rapidly sample inputs from the surrounding environment and construct a seemingly coherent and stable perceptual representation of the world [1,2]. Visual sampling occurs through fast-paced sequential eye movements (e.g., several saccades/second), which interrupt the continuous stream of incoming visual input [3]. To correct for consequential undesired impressions of apparent perceptual motion due to retinal shifts, the visual system leverages compensatory perceptual mechanisms which integrate information

across *externally* and *internally* generated signals [4–7]. In the brain, externally generated, largely sensory, signals must be distinguished from internally-generated signals, which are theorized to arise from internal models based on the copies of issued motor commands (i.e., corollary discharges) [1,8–11].

During moments in which saccades are being executed, it has been observed that subjects often fail to notice changes in the location of objects, particularly if such changes are small. This phenomenon has been referred to as saccadic suppression of displacement (SSD) and has been attributed to the brain's decreased perceptual sensitivity around the time of the saccade [12]. In addition, seminal findings by Bridgeman (1975) [13] and Westheimer (1984) [14] found that retinal acuity tended to decrease as a function of saccades' eccentricity. Based on Bayesian models of trans-saccadic integration, these results have been recontextualized as optimal inference mechanisms whereby the brain may be maintaining a sense of spatial constancy by pooling information from at least three signals: retinal locations, velocity signals, and a proprioceptive sense of the eye position [15–17]. Such optimal integration has also been determined to occur despite occasional masking of sensory information, for instance when a visual target is briefly removed from the screen following a saccade and subsequently reappears in a new location (i.e., blanking) [17]. In order to achieve integration at the time of saccades, previous research suggests that the brain may be estimating causal relationships between presaccadic and postsaccadic visual representations [17,18].

Understanding the precise mechanistic process underlying visual integration between foveal and extraretinal signals across saccadic (sampling) shifts requires one to understand how perception is impacted by the magnitude of the saccade amplitude and extent SSD might be impacted by visual objects' retinal shifts. In that regard, the displacement detection task used by

Bridgeman et al (1975) [13] provides an excellent paradigm through which to study the different dimensions of this perceptual process. In this task, participants are asked to execute saccadic eye movements in response to a peripheral target that follows a central fixation period. While participants make the saccade, the target is extinguished and reappears at a slightly shifted location (i.e., displacement). Subjects then report the perceived direction of the target shift that follows the saccadic eye movement [13,19–21].

In addition to standard behavioral measurements as applied by the above studies to capture perceptual biases, one can investigate participants' perceptual judgments with mathematical models. One common class of model is Signal Detection Theory (SDT) [22], which estimates a distance measure of sensitivity between hits and false alarms as part of mathematical distributions and expresses such distance in terms of *d'*. This technique offers meaningful insights in the form of response distributions and has often been used to capture decision-making and perceptual processes [23]. Other techniques have focused instead on psychometric profiles based on participants' responses, which have provided measures of perceptual sensitivity (i.e., smallest displacement detected greater than chance) and bias (i.e., reported target shift corresponding to chance level) [21,24,25]. Using such psychometric measures, previous analyses pertaining to the displacement detection task have shown that larger target shifts were easier to detect than smaller shifts [21,25].

While SDT and psychometric mathematical representations of perceptual judgments can provide important and meaningful perceptual insights, they do not account for the holistic decision-making process unfolding over time leading to such responses, focusing instead on the responses resulting from perceptual judgment. As an alternative approach, one can leverage a computational framework such as the drift diffusion model (DDM) to gain insight into the

perceptually-based decision-making process [23,26–29]. One advantage of the DDM is that it can both model choice and reaction time data, and it can thus more holistically capture the decision-making process [23,28,29]. The model has been argued to act as a dynamic extension of the SDT framework [22,28] through the simulation of an evidence accumulation process whereby one iteratively "samples" decision steps from either one of two choice distributions. In doing so, the DDM captures an additional temporal dimension that affords a mechanistic explanation of reaction times in perceptual tasks such as the displacement detection task described above. In the literature, the DDM has successfully accounted for decision processes across a wide variety of experimental settings including perceptual decisions [30], working memory processes [31,32], social decisions [33], and value-based decisions [34–38].

One gap in the literature is to understand *how* and *when* perceptual, or externally-generated, signals lead to perceptual judgment alterations. In that regard, DDM simulations provide an explanatory framework with respect to the process dimensions that may have been impacted by perception [23,39]. For the purposes of the current study, we aimed to computationally connect saccadic eye movement metrics to perceptual decisions. Often, saccades fall short of the intended visual targets [40,41]. In such cases, a small target shift in the direction of the eye endpoint location would result in close retinal proximity, which based on our knowledge of SSD would likely decrease perceptual sensitivity. Thus, we hypothesized that perceptual errors would predict a greater biasing effect for smaller target shifts.

The objective of this work is to leverage the displacement detection task and the DDM modeling framework [31] to characterize the evidence accumulation process unfolding over time leading to perceptual decisions represented by decision boundaries. The DDM posits that this is a noisy process and that decision-making can be measured in terms of decision speed and response

accuracy [27,42–44]. We aimed here to capture the biasing effects pertaining to perceptual errors that altered the evidence accumulation process resulting in perceptual judgments. We operationalized perceptual errors in terms of visuospatial offsets relative to visual targets. We hypothesized that such errors could be used alongside perceptual choice data to account for decision-making biases with the DDM. We introduce a novel statistical framework that directly connects perceptual errors to perceptual judgment accuracy in the form of coefficient weights; we then quantify the offset in terms of evidence accumulation relative to such coefficients. We show how this approach captures individual asymmetric patterns in terms of choice (i.e., decision) and reaction time profiles. Our DDM-based framework may later provide a computational basis for investigating the precise neural basis of perceptual biases in visual perception decision-making.

Materials and Methods

Participants

Thirty healthy participants between the ages of 18 and 41 years-old (*M* = 22.57 years-old; *SD* = 5.17 years) took part in this study. Twenty-one participants were female, and 9 participants were male. All had normal or corrected vision. Informed consent was obtained from every participant and study protocols were approved by the Institutional Review Board at the University of California, Davis. All study procedures were conducted at the UC Davis Imaging Research Center in Sacramento, California.

Apparatus

Participants were seated in a darkened room with their head stabilized by a chin and forehead rest, 100 cm in front of a 1980 x 1200 Dell U2415 monitor with 60 Hz refresh rate (Dell Technologies Inc., Round Rock, TX). Manual choices were registered on a button box at the desk.

Fixations and saccades of the right eye were recorded with the Eyelink II eye tracker (head-mounted binocular eye tracker, 1000 Hz temporal resolution, 0.01° spatial resolution, Eyelink CL version 5.15 source, Eyelink GL camera version 1.2; SR Research Ltd., Mississauga, ON, Canada) and E-Prime 2 software (Psychology Software Tools Inc., Sharpsburg, PA). Stimulus presentation and manual button box response data were acquired in E-Prime 2. Stimuli presented were either a black fixation cross or a filled black circular target on a gray background. At the start of the experiment, a five-point calibration and validation were performed.

Task and Procedure

The task was adapted from a previous trans-saccadic visual perception experiment [45]. At the beginning of each trial, a fixation cross (0.3° in extent & 8.5 mm height and width) was presented at the center of the screen. Participants held their gaze on the cross for a random duration between 1200 and 1800 ms. A circular initial target (with a 8.5 mm pixel diameter) appeared in either the left or right direction from fixation and required a saccade of amplitude 4° or 8°. As soon as the eye-tracker determined that participants' eye position was no longer in a 3.2° square window centered on the fixation cross, the target disappeared (i.e., blank screen) for a time period of 250 ms, and subsequently reappeared at one of 11 shifted locations ranging between - 2.50° and + 2.50° (see Fig 1A).

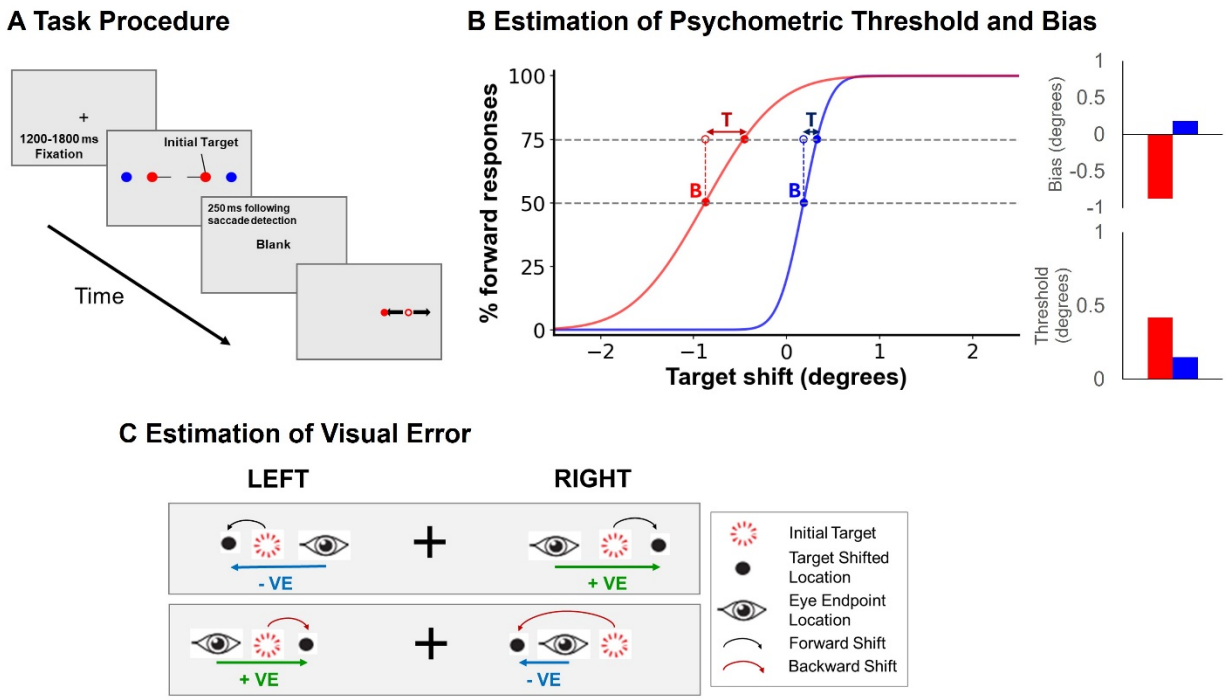

Fig 1. Description of the trans-saccadic shift detection task.

(A) Overview of the task procedure. Trials started with a fixation cross. An initial target then appeared on either the left or right side of the screen and required a 4° or an 8° saccadic eye movement. Following a 250 ms blank screen, the target reappeared at a shifted position ranging from 2.5° to the left to 2.5° to the right. (B) Overview of the psychometric threshold and bias. The proportion of forward button press responses is plotted against the target shift magnitude. Button press responses were fitted with a beta binomial model to determine the psychometric function which were the basis of the psychometric bias and psychometric threshold. The psychometric bias (indicated with a 'B') corresponds to the point on the curve at which there were 50% forward responses. The psychometric threshold (indicated with a 'T'), on the other hand, corresponds to the step, in degrees, that is required to go from 50 % forward responses to 75% forward responses. On the plot, the red curve corresponds to an example psychometric function with a negative bias and a high threshold. The blue curve, on the other hand,

corresponds to an example psychometric function with a slightly positive bias and a low threshold. (C) Visual error (VE) description. A target shift could take place in the forward direction (i.e., away from the fixation cross; black curved arrow) or it could take place in the backward direction (i.e., back towards the fixation cross; red curved arrow). The VE indicates the difference between the eye position and the shifted target position. A positive VE, indicated in green, corresponds to a case in which the shifted target lies to the right of the eye. A negative VE, indicated in blue, corresponds to a case in which the shifted target lies to the left of the eye.

Target shifts were uniformly distributed across non-zero shifts, and there were twice as many trials that did not involve any visual displacement of the initial target (i.e., zero shift) relative to non-zero shifts. In the experiment, we contrasted forward vs. backward target shifts. Forward shifts refer to visual targets that reappeared further away from the fixation cross. Backward shifts refer to the visual targets that reappeared closer to the fixation cross (see Fig 1C for illustration of forward (top panel) and backward shifts (bottom panel)). Across all blocks, there were 80 instances of zero shifts, and 40 instances of each of the 10 non-zero target shifts. For each target shift, half of the trials involved initial targets appearing to the left or right of the fixation cross, and half of the trials required 4° or 8° saccades. Participants were instructed to make a manual decision (‘left’ or ‘right’ labeled buttons) to indicate the target shift direction as quickly as possible, without sacrificing accuracy. Forward responses refer to button presses whose indicated direction (‘left’/‘right’) was *congruent* with the initial saccade direction (‘left’/‘right’) and are mathematically represented with a positive angle (in °). Conversely, backward responses refer to button presses whose indicated direction was *incongruent* with the initial saccade direction and are mathematically represented with a negative angle (in °). Target shifts ranged from -2.50° to +2.50°

and were uniformly distributed except for the zero target shift that was occurred twice as frequently (see target shift axis on Fig 2 and 4).

Prior to the start of the experiment, participants were given three attempts at a 10-trial practice run to familiarize themselves with the task. Target shift magnitudes from the practice run had the same frequency distribution as the main experimental trials. Overall, feedback on task accuracy was provided at the end of each practice run, but no feedback was provided after trials from any of the 10 blocks. There were 480 collected trials throughout the experiment (48 trials separated into 10 blocks). The task lasted 30 minutes on average.

Experimental Design and Statistical Analysis

Accounting for decision-making in the trans-saccadic task can be done through an analysis pipeline consisting of three main steps (see Fig S1 for flowchart): The first step is to extract the relevant experimental measures from the task. These include the amplitude (in °) of the jump size, the visual error, and the manual choice. One can enter these three measures into a linear model to predict response accuracy based on the visual error, while controlling for trials' jump sizes (see Fig 2 and Fig S1). In doing so, linear weights pertaining to the error can be estimated to capture perceptual biasing effects on decision-making (i.e., vector of VE βs). Such coefficients are then input into a matrix (Fig 4) to simulate the offset in the DDM's drift rate, which is directly proportional to the corresponding target shifts' VE βs (Fig 5C). See Fig S1 for a comprehensive illustration of all such steps.

Behavioral measures

A measure of accuracy was computed for each trial of every block. Accurate responses consisted of button presses whose indicated direction ('left' and 'right') matched the target shift

direction ('left' vs. 'right'), and were coded with a 1 whereas inaccurate responses were coded with a 0. This coding was used for later modeling purposes. In the case of the 0 target shift, either button press was considered correct (and coded with a 1) since no target shift occurred. Choice data were computed in terms of % forward responses (based on participants' button presses) relative to the total number of trials for that target shift direction and amplitude. We reported the group mean accuracy (%) and standard error of the means across all target shifts for trials involving a saccadic eye movement of 4° and 8° amplitudes separately.

A measure of reaction time (RT) was also calculated for every trial to indicate the time required for participants to respond to a target shift (in ms). This time was the interval between when the target reappeared and the button press timing onset. We first computed the mean manual reaction time across trials with zero target shift, and reported the reaction time at all other target shifts in terms of a percentage relative to the zero target shift reaction time. Zero target shifts represent the case in which participants had to guess because the target neither moved to the left nor to the right. Normalization of reactions times by the zero target shift was carried out within subjects. We reported the group mean manual reaction time (%) and standard error of the means across all target shifts for trials involving a saccadic eye movement of 4° and 8° amplitude separately.

Psychometric analyses

In order to capture participants' response profiles across target shifts, we characterized participants' perceptual sensitivity to target shifts with psychometric curves and a posterior distribution estimated with Bayesian methods and a beta-binomial model fitted to manual choice (proportion of forward responses) [46]. This method specifically required estimating five parameters: namely the *threshold*, the *width,* the *lapse rate*, the *guess rate,* and an *overdispersion*

238 parameter [46]. In terms of the psychometric curve itself, psychometric sensitivity was quantified
239 in terms of the percentage of forward responses as a function of the target shift (see Fig 1B). Two
240 measures were extracted from individual participants' psychometric curves—the *psychometric*
241 *bias* and the *psychometric threshold* (see Fig 1B for illustration of both).

242 Specifically, the psychometric bias (labeled with a 'B' on Fig 1B) corresponds to the point at
243 which the participant reported that the target jumped forward 50% of the time (i.e., at chance level).
244 A positive psychometric bias indicates that the participant tended to report backward responses for
245 small forward target shift. The blue curve in Fig 1B illustrates an example of a slight positive
246 psychometric bias. Conversely, a negative psychometric bias indicates that participants tended to
247 report forward responses for small backward target shifts. The red curve in Fig 1B illustrates an
248 example of a negative psychometric bias.

249 The psychometric threshold (labeled with a 'T' on Fig 1B) corresponds to the target shift
250 difference (or step) required to transition from 50% forward responses to 75% forward responses.
251 This measure corresponds to a participant's difficulty in perceiving trans-saccadic shifts. The
252 psychometric threshold tends to be highest when participants make numerous erroneous responses
253 at the transition point between backward and forward target shifts, thus resulting in a flatter
254 psychometric curve and indicating low perceptual sensitivity in detecting the target shift direction.
255 This corresponds to the red psychometric curve on Fig 1B. Conversely, the psychometric threshold
256 tends to be lowest when participants make very few erroneous responses at the transition point,
257 thus resulting in a steeper psychometric curve and indicating high perceptual sensitivity in target
258 shift detection. This corresponds to the blue psychometric curve on Fig 1B. In MATLAB,
259 psychometric functions were fit with the *psignifit* function [46].

260

Saccadic and visual error measures

Perception was only assessed in the horizontal plane as previous research has shown that there are no significant trans-saccadic perceptual differences between horizontal and vertical movements [21]. Successful trials required a detectable initial saccade (eye velocity exceeding 50°/s and acceleration exceeding 8000°/s²) and a response between 200 ms and 1,200 ms of the shifted target's appearance [47,48]. Saccade initiation was detected when the eye position exited the fixation window. Included saccades were all initiated within the fixation window, had a saccade timing onset within 300 ms after the appearance of the first target, with valid eye fixations, based on the eye tracker, at the time of the target shift reappearance. In addition, we computed the gain to quantify the amount subjects undershot or overshot the initial target. Saccade gain was calculated relative to the target in terms of the location of the initial saccade and the initial target location (see equation 1).

$$Gain = \left[(fixation - target)/target\right] \times 100\% \quad (1)$$

Overshoots were defined as saccades whose gain exceeded 100% and undershoots were defined as saccades whose gain was lower than 100%.

A visual error (VE) corresponds to the difference between the eye endpoint location and the shifted target location. It measures the visual offset relative to the target after a target shift. Specifically, this distance was quantified by taking the vector magnitude, in visual angle, between the eye position at the shifted target reappearance time and the shifted target location along the horizontal axis. The VE's sign indicates the position of the eye fixation relative to the shifted target. A positive VE occurred when the target's shifted location was to the right of the eye endpoint location (Fig 1C, top right and bottom left). A negative VE occurred when the target's shifted location was to the left of the eye endpoint location (Fig 1C, top left and bottom right).

Encoding the VE in the left-right direction was done for linear modeling purposes (see "Linear modeling analyses" section below) to predict response accuracy from the VE and cancel out cases in which the VE was perfectly symmetric across leftward and rightward saccades.

In order to get an insight into the specific target shifts at which there was a discrepancy between the shift's direction and the VE, we computed the VE-shift congruency in terms of sign consistency across the target shift and the VE. Specifically, the expectation in terms of congruency was that a visual target being shifted to the left would result in a negative VE relative to the eye endpoint location (see Fig 1). Conversely, a visual target being shifted to the right would be expected to result in a positive VE relative to the eye endpoint location. For each target shift, we calculated the % VE-shift congruency in terms of the proportion of trials that resulted in this expected sign congruency relative to all trials at that specific target shift. We did this separately across saccade amplitudes of 4° and 8°.

In order to capture the perceptual progression across negative and positive target shifts from backward VEs to forward VEs, we turned the VE into a signed measure across all trials by dividing each VE by its absolute value (i.e., $\forall\, x \in \mathbb{R}^*, sgn(x) = x/|x|$), except when the VE was 0° in which case sgn(0)=0. For each target shift, each saccade amplitude (4° and 8°), and each saccade direction (leftward vs. rightward saccades), all VE signed measures had possible values within {-1,0,+1}. We then computed the proportion of backward vs. forward VEs in the [-1,1] range by computing the following measure (see equation 2).

$$VE_{F|B} = \left[\mu(sgn(\boldsymbol{VE_{Right}}))/2\right] - [\mu(sgn(\boldsymbol{VE_{Left}}))/2] \quad (2)$$

where μ indicates the mean, $\boldsymbol{VE_{Right}}$ refers to the vector of VEs resulting from a rightward saccade, and $\boldsymbol{VE_{Left}}$ refers to the vector of VEs resulting from a leftward saccade. Dividing each of the two means by 2 ensures that the total stays within the [-1,1] range, and subtracting the leftward VE

sign encodings translates the VE into a forward vs. backward directed vector. More precisely, here a value of -1 indicates cases in which all VEs were estimated in the backwards direction, and a value of +1 indicates cases in which all VEs were estimated in the forward direction. To characterize the progressive switch from -1 to +1, we fit all $VE_{F|B}$ proportions across target shifts at the individual and group level by considering a logistic function fit $f(x)$, which was defined as follows (see equation 3).

$$f(x) = \frac{2}{1+\exp\left(-k\cdot(x-x_0)\right)} - 1 \quad (3)$$

where k refers to the growth rate (higher k indicates a faster switch), x_0 refers to the inflection point, 2 is the range, and -1 is the fixed intercept to ensure the function ranges from -1 and 1 as its two fixed asymptotes. In this experiment, we were particularly interested in estimating x_0 as a measure of VE bias.

Linear modeling analyses

We next wanted to use a single model to incorporate the information pertaining to the VE with the response profiles across target shifts. To achieve our goal of capturing perceptual biasing effects on decision-making, we used the estimated parameters of a linear model as an additional input to the DDM. Mainly, the linear model provided weights assigned to VEs across all target shifts, which predicted participants' accuracy in their perceptual responses. Fig 2 shows a visual illustration of the linear modeling procedure. The main objective was to predict participants' manual choice accuracy (encoded with 1's to represent correct responses and 0's to represent incorrect responses) based on the visual error sorted by target shift. Note that we also added two separate intercepts based on the original magnitude of the initial saccadic eye movement. One was estimated for saccades with a magnitude of 4° and one for saccades with a magnitude of 8° (240

trials for each). The model allows one to statistically infer a relationship between direction and size of the visual error, and the resulting manual report response accuracy (see Fig 2). Eleven individual βs were estimated across all shifts and are shown on the target shift axis to the right of β weights on Fig 2. The VE β corresponds to a linear weight on the target shift's VE to quantitatively estimate the degree to which VE can predict manual choice accuracy.

In MATLAB, we estimated the vector of 11 βs (shown in blue on Fig 2) across all trials simultaneously. We used the syntax $\boldsymbol{\beta} = \boldsymbol{X}\backslash\boldsymbol{Y}$ where **Y** is the accuracy vector across all 480 trials, $\boldsymbol{\beta}$ is the vector of 13 βs, and **X** is the 480 x 13 matrix including binary encodings for X_{amp4} and X_{amp8}, ("amplitude" columns shown in black and red, along with their corresponding β_1 and β_2 weights shown in magenta on Fig 2) as well as the VE or 0 encodings for all other target shift Xs $X_{ts=-2.5}$ through $X_{ts=2.5}$ (last 11 columns shown in black and purple, along with their corresponding βs, β_3 through β_{13}, shown in blue on Fig 2). We focused our analyses on the VE βs (β_3 through β_{13}) which indicate the extent VE is predictive of manual choice accuracy, and if so, whether it predicts a correct response. More specifically, sign *congruency* between VE and the βs means that a VE with greater magnitude is predictive of more accurate manual choice, whereas sign *incongruency* between VE and the βs means that the VEs are less predictive of correct manual choices. The strength of this predictive effect is determined by the magnitude of the VE β and the corresponding number of correct manual choices that are being predicted. To estimate variability in the vector of VE βs at the individual level, we applied an additional bootstrapping step. Such step involved sampling trial data (i.e., 480 trials in the matrix) with replacement and refitting the VE β coefficients with the same linear model based on resampled data. Bootstrapping was repeated 2,000 times and each yielded a new vector of 11 VE βs corresponding to each target shift. For each target shift, we used the distribution of all 2,000 βs at specific shifts to estimate the

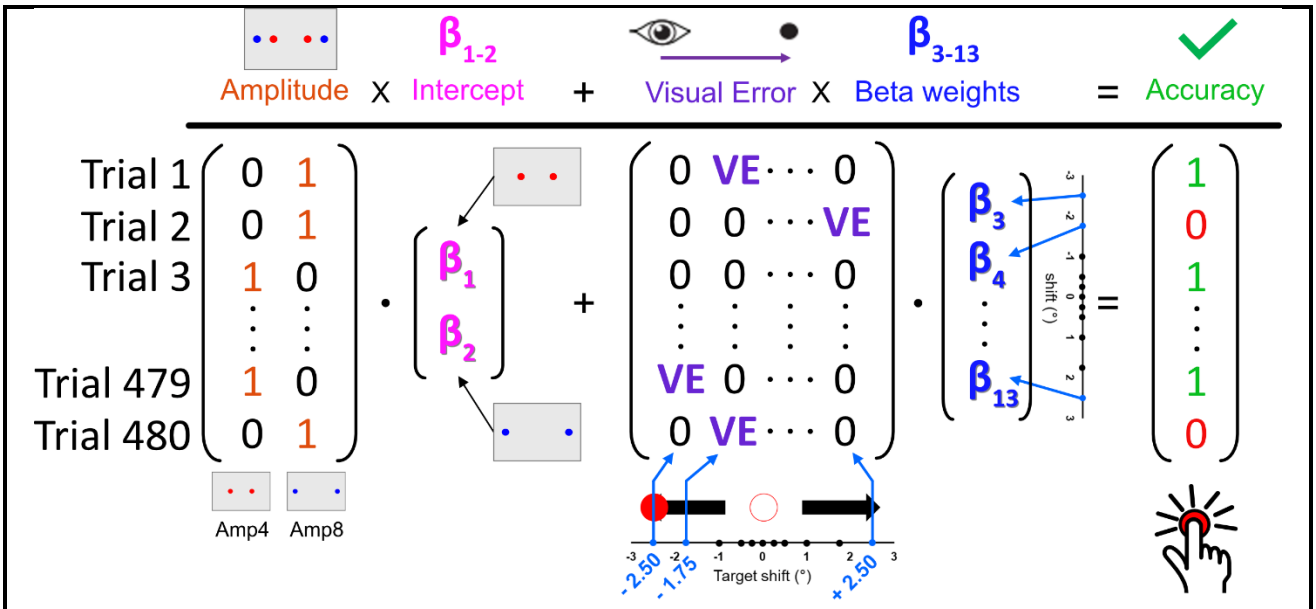

Fig 2. Visual illustration of the VE linear modeling framework.

Manual choice accuracy is predicted based on the amplitude of the initial saccadic eye movement and the visual error at a specific target shift. Beta weights are estimated across all 480 trials using multiple linear regression. The manual choice (dependent variable) is encoded with 1's to indicate correct responses and 0's to indicate incorrect responses. The saccade amplitude is encoded in terms of a binary variable with 1's indicating the current trial's required eye movement. Single intercepts β_1 and β_2 are estimated across all trials occurring with saccades of amplitude 4° and amplitude 8° respectively. The main independent variable is the visual error, spread out across target shifts. For each target shift, a single β is estimated based on the visual error from all trials occurring at that specific target shift. These VE β are later used to quantify the lateral bias (equation 4).

standard deviation across all 2,000 estimations. We reported this as our variability measure at the individual level.

In this experiment, note that 240 trials involved initial saccades to the *left* of the fixation cross and 240 trials involved initial saccades to the *right* of the fixation cross. To reiterate, the VE is

defined with sign consistency across leftward and rightward saccades, which means that a negative VE always indicates that the shifted target has reappeared to the left of the eye fixation location and a positive VE always indicates that the shifted target has reappeared to the right of the eye fixation location, regardless of the direction of the initial saccadic eye movement. However, since the signs of the forward vs. backward target shifts opposed one another across leftward vs. rightward saccades, this means that their corresponding VEs also had opposite signs. For any given target shift, a VE β approximating 0 would indicate symmetric VEs across leftward vs. rightward saccades whereas a VE β significantly different from 0 would indicate an asymmetry in VE across leftward vs. rightward saccades. Specifically, sign consistency across VEs from leftward and rightward saccades leading to correct trials with *negative* VE βs would indicate that the visual target tended to reappear further to the *left* of the eye in such correct trials, whereas sign consistency across VEs from leftward and rightward saccades leading to correct trials with *positive* VE βs would indicate that the visual target tended to reappear further to the *right* of the eye in such correct trials.

Therefore, one can think of the vector of VE βs as a vector of asymmetric VE biases across target shifts. Based on such biases and for each participant, one can then quantify the overall lateral bias across target shifts in terms of the center of gravity of the vector of absolute VE βs as follows (see equation 4).

$$lateral\ bias = \sum_{s=shifts} s \times |\beta_{VE(s)}| \quad (4)$$

Mathematically, the lateral bias indicates visual errors' bias center of gravity, or in other words, the extent to which the VEs bias decision making in the forward vs. backward direction. According to this framework, a negative lateral bias would indicate a greater propensity towards

perceptual asymmetry in the backward direction whereas a positive lateral bias would indicate a greater propensity towards perceptual asymmetry in the forward direction.

General description of the drift diffusion model (DDM)

Three different versions of the DDM were fitted to the choice (% forward responses) and manual reaction time (RT) data across target shifts (see Fig 3 for illustration of the DDM). DDM model inputs consisted of an 11 x 8 matrix, which included the target shifts (1st column), the forward and backward manual reaction time means and standard error of the means (columns 2-5), the number of forward responses (column 6), and the total number of trials corresponding to a given target shift (column 7). An eighth column was added to the input matrix as a VE β estimate for each target shift. This column corresponded to the VE βs (i.e., β_3 through β_{13}) in the linear model predicting accuracy as described above (see Fig 2). Note that such VE β inputs were only incorporated into the DDM in the asymmetric (hybrid) version of the model which we define later in more detail. See Fig 4 for an illustration for the DDM input matrix.

The model progressively accumulates momentary evidence towards an upper ("A") or lower bound ("B"; see Fig 3). Each bound indicates one out of two possible choice options (i.e., "left" vs. "right" target shift report). Positive evidence leads to a greater probability of selecting choice "A", whereas negative evidence leads to a greater probability of selecting choice "B". Evidence accumulated at each time step is drawn from a unit-variance Gaussian distribution with mean set by the drift rate (DR), which we designate r in the equations below. The DR for any given trial is a linear function of the stimulus input. We employ three versions of the DDM described in more detail below. For two of these versions, the stimulus input is simply the target shift; for the other,

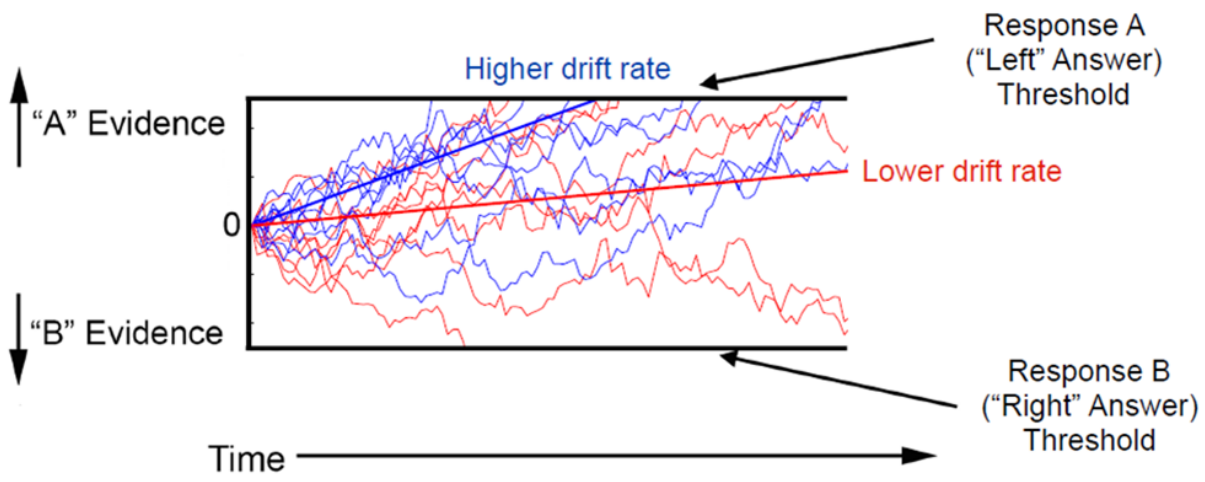

Fig 3. Visual representation of the drift diffusion model (DDM) and drift rate (DR). The DDM represents the information accumulation process that unfolds during decision-making, and is modeled as a function of the signal-to-noise ratio of information gathering towards the decision point, a decision bound for making a decision, and non-decision time (due to motor processing). The DR is the average slope of evidence accumulation (represented with solid lines). On this diagram, "A" and "B" correspond to each of the two possible shift directions ('left' and 'right').

the stimulus input also incorporates the VE. In either case, a single parameter that we call the DR coefficient scales the stimulus input into a DR for the corresponding trial. The decision bound that is first reached indicates the choice that is selected ("A" vs. "B"), and the corresponding decision time is determined by how long it took the DDM to pass the decision threshold. For the purposes of these computational simulations, the DDM was run within-subjects across all target shifts for all trials corresponding to a given saccadic eye movement amplitude (4° vs. 8° trials).

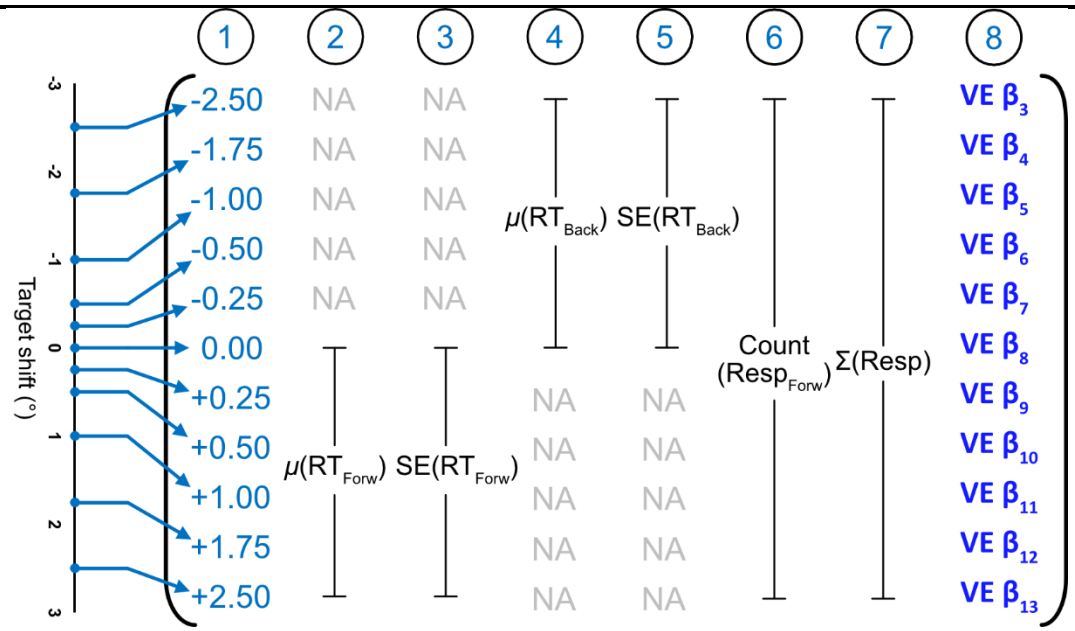

Fig 4. Visual representation of the DDM input matrix.

Data pertaining to the target shifts, reaction time, manual choices, and VE βs were entered into an input matrix, and were the basis of DDM analyses. In this matrix, each of the 11 rows corresponded to trials with different target shifts. There were a total of 8 columns. The first column indicated the target shift. The second and fourth columns indicated the mean manual reaction time across forward trials (2nd column) and backward trials (4th column). The third and fifth columns indicated the manual reaction time standard errors across forward (3rd column) and backward trials (5th trials). The sixth and seventh columns indicated the total number of forward responses and the total number of responses respectively. The eighth column indicated the VE βs that were estimated as VE weights across target shifts based on the earlier linear model (Fig 2).

Mathematically, the probability of exceeding the decision threshold A before B is represented by the following equation (see equation 5).

$$P_a(r,A,B) = \frac{e^{2rB}-1}{e^{2rB}-e^{-2rA}} \quad (5)$$

The mean time (T) to bound A is represented by the following equation (see equation 6).

$$< T_{a(r)}(r,A,B) > \; = \frac{A+B}{r}\coth\left((A+B)r\right) \quad (6)$$

In this study, the decision time mostly depended on three parameters: DR coefficient, decision bound, and non-decision time [27,42,44]. The DR coefficient and decision bound were estimated in a proportional manner relative to the magnitude (i.e., absolute value) and direction (i.e., sign corresponding to forward/backward) of the target shifts. Overall, the DR coefficient provides an index of trial difficulty with higher DR coefficients corresponding to faster responses. The decision bound indicates the tradeoff between speed and accuracy with higher bounds corresponding to slower decisions, and the non-decision time parameter estimates the time that was not spent accumulating evidence during decision making and is assumed to account for sensory and motor latencies. In the computational implementation of the DDM, both parameters were computed relative to the stimulus target shift input. The non-decision time, on the other hand, was estimated as a single constant for all shifts with initial 4° vs. 8° saccadic eye movements. All parameters were fit by computationally minimizing the negative log likelihood of the data (i.e., maximizing likelihood of data) [44].

The baseline DDM assumed symmetry across the two decision bounds "A" and "B" (see Fig 5A). This means that for each target shift s, the time to reach the corresponding forward decision threshold "A" matched the time to reach the corresponding backward decision threshold "B" for target shift -s, or in other terms, $T_{+s(a)} = T_{-s(b)}$ where A = -B. The second DDM matched the baseline DDM structure, but additionally incorporated a bias term which violated the assumption of symmetry from the first model. The DDM bias represents an initial offset that favored one of the two possible decisions by shifting the decision bounds in the forward or backward direction.

In the second model, the bias was quantified by the extent to which the starting point (0 point on Fig 3 & Fig 5) was shifted upwards towards the "A" decision bound (i.e., positive bias), or downwards towards the "B" decision bound (i.e., negative bias; see Fig 5B for an illustration of a downwards bias).

Decision-making bias accounted for by and based on VE β

To test whether our measures of perceptual asymmetry across target shifts (VE β) could fully capture the decision-making process unfolding over time, we estimated participants' reaction time profiles based on the VE βs as part of two separate linear mixed-effects models (LMEM). In both models, we set up the measure of VE β as the main fixed predictor and added three random intercepts to account for variability across participants, saccade amplitudes, and target shifts. The first LMEM used the RTs from the uniform (baseline) DDM as the dependent variable (see Fig 5A), and the second LMEM used the RTs from the DDM with a bias estimate as the dependent variable (see Fig 5B). Both LMEMs were defined according to the following equation:$Y_{RT} = \gamma_1 X_{VE\beta} + Z1_{subject} + Z2_{Amplitude} + Z3_{TargetShift}$. In R, we imported and utilized functions from the lme4 [49] and lmerTest packages [50] to fit the linear mixed-effects model. The model was written as lmer(RT ~ VE_β + (1|subject) + (1|amplitude) + (1|target_shift)). The restricted maximum likelihood (REML) technique was employed to fit each model and we obtained p-values for each β estimate. We also reported the 95% confidence interval around the γ_1 coefficients corresponding to VE β by running the 'confint' *R* function with the Wald method.

To tie the DDM's biasing effect to perceptual asymmetry, we designed a third integrative DDM that input the vector of VE βs estimated from linear modeling analyses (see Fig 2 and 8th

column of Fig 4). We additionally estimated a fifth DDM parameter *w* that scaled the biasing contribution of the VEs on the DR (see Fig 5C). For each target shift, the inputs to the DDM were

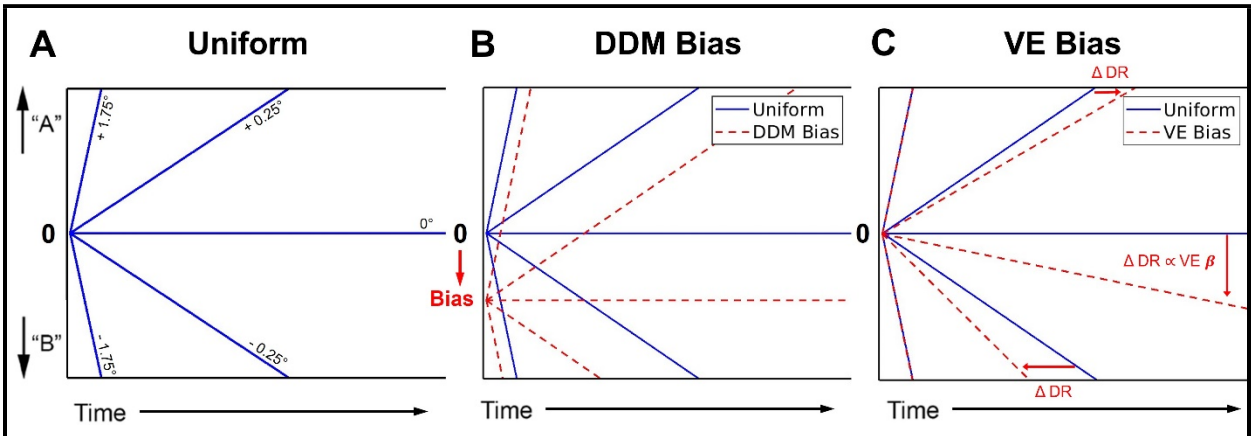

Fig 5. Visual representation of the DDM models with or without a bias.

(A) The baseline DDM corresponded to a uniform case in which the drift rates were perfectly symmetric across the backward and forward directions. Straight lines correspond to average evidence accumulation trajectories. (B) There were two ways a bias could be introduced in the model. The first way is through a general bias which consisted of an inherent shift of the DDM starting point. Straight blue lines correspond to uniform drift rates. Red dashed lines correspond to biased drift rates. (C) The second way is through a drift rate bias that is proportional to the VE β at individual target shifts. Straight blue lines correspond to uniform drift rates. Red dashed lines correspond to biased drift rates

quantitatively assessed as $input = s + w \times \beta_s$ where *s* indicates a target shift and β_s denotes the corresponding VE β. Since each target shift's drift rate was directly proportional to its corresponding VE β, this resulted in a shift of the DR as shown on Fig 5C. Note that there were unique *w*'s (i.e., DDM VE β weight, or DDM-based VE bias scaling factor) for each of the 4° and

8° trials. Therefore, trials without any bias (i.e., $\beta_s = 0$) would result in the input being equated with the target shift.

Conversely, trials with non-zero biases would result in the input being biased proportionally based on the sign and magnitude of the vector of VE biases β_s. All DDM parameter estimates were used to simulate a second DDM-based psychometric function and manual reaction time profile across target shifts. Note that the DDM assumed that the reaction time would consistently increase as the target shift decreased and choice data would be characterized by greater error rates for small target shifts relative to larger target shifts. Such assumptions happened to be violated on occasion in instances where participants either made very few mistakes (i.e., step function) or made no mistakes in one direction but many mistakes in the other. See S1 Appendix for more details.

We considered standard model fit estimations in terms of the Bayesian Information Criterion (BIC) across the psychometric and DDM forward response profiles, which was computed as follows (see equation 7).

$$BIC = N_s \times ln\left(\frac{RSS}{N_s}\right)k \times \ln(N_s) \tag{7}$$

where k refers to the number of estimated parameters (i.e., 5 for both models), N_s refers to the total number of target shifts (i.e., $N_s = 11$; see Figs 2 and 4), and RSS refers to the residual sum of squares between the estimated and empirically collected observations. Statistically, the model with the best fit to the data corresponds to the model that yields the lowest BIC value. To compare the DDM BIC and beta binomial BIC across psychometric fits, we utilized a paired t-test on participants' BIC measures across trials with 4° and 8° saccade jumps.

Other statistical analyses

All statistical analyses were performed in *R* version 4.1.3. For psychometric analyses, paired *t*-tests were performed on the estimated psychometric bias and threshold across saccades with amplitude 4° and 8°. To test for potential differences in response accuracy, reaction time, and shift-VE congruency levels, we applied a 2x11 two-way analysis of variance (ANOVA) with repeated-measures and a Greenhouse Geisser correction. The factors were the saccade amplitude (4° and 8°) and target shift (11 possible shifts). For each ANOVA, and depending on significance levels, post-hoc pairwise *t*-tests were used with a Bonferroni correction. For the VE gain measure, a 2x2 two-way analysis of variance (ANOVA) with repeated measures and a Greenhouse Geisser correction was applied with saccade amplitude (4° and 8°) and gain type (undershoot vs. overshoot) as the two factors. To test for VE bias differences saccade amplitudes, we used a paired *t*-test on the group logistic fits' inflection point x_0 across trials with 4° vs. 8° saccade jumps.

To test for potential relationships between the lateral bias estimated with the linear modeling technique described above and other measures, we utilized Pearson correlations (r) to assess participants' correspondence between the lateral bias and the VE inflection point (x_0), the psychometric bias, and response accuracy. The correlation with the VE inflection point was used to relate the lateral bias to known VE effects that are inherently perceptual. The correlation with the psychometric bias was used to relate the lateral bias to known psychometric effects based on the response measures only. The correlation with response accuracy was used to relate VE-based biases to participants' accuracy level in the trans-saccadic task. Finally, we applied a final Pearson correlation (r) to explicitly relate the lateral bias to the DDM-based VE β weight estimated across 4° vs. 8° saccade jumps (i.e., based on the hybrid version of the DDM). This latter correlation was

used to link the VE-based bias to the evidence accumulation process unfolding over time, as simulated by the DDM.

Results

The main objective of this paper is to use the DDM computational modeling framework in the context of the displacement detection task to characterize the evidence accumulation process leading to perceptual judgments (i.e., based on manual choices). We introduce a linear modeling technique whose purpose is to estimate visual error coefficients that can subsequently be used in the DDM to capture the perceptual bias on decision-making. We aimed to assess to what extent the DDM can simulate participants' choice and reaction time psychometric profiles relative to other techniques such as the beta binomial model that simulates choice data. Overall, we show how the DDM technique can capture individual asymmetric perceptual judgment patterns by accounting for visual biases.

Psychometric and Manual Choice Measures

Fig 6 presents the behavioral results from the visual perception task. Psychometric curves were fitted to individuals' proportions of forward responses across target shifts. Although the average psychometric bias estimate was close to 0, we noticed that there was some between-subject variability, with more spread across participants in the 8° condition. No significant differences across 4° and 8° group mean biases were found, t (29) = 1.50, p = 0.14. In terms of the psychometric threshold, there was a significantly larger threshold for the 8° trials compared to the 4° trials, t (29) = 7.40, $p < 0.001$. Consistent with previous work [21,51], this result indicates lower sensitivity in the detection of target shifts for larger saccades.

A two-way analysis of variance (ANOVA) with repeated-measures and Greenhouse Geisser correction was performed to evaluate the effects of saccade amplitude (4° and 8°) and target shift (11 possible shifts) on response accuracy. ANOVA results pertaining to response accuracy are reported in Table 1. The main effect of saccade amplitude was due to a greater proportion of accurate responses following small saccade jumps (4° M = 94.02 %, SE = 2.09) relative to large saccade jumps (8° M = 90.15 %, SE = 3.05). There was also a main effect of target shift mainly driven by progressively smaller proportions of correct responses for short target shifts (e.g., -0.25° M = 84.16 %, SE = 3.97; +0.25° M = 79.04 %, SE = 3.46) relative to long target shifts (e.g., -2.50° M = 98.30 %, SE = 0.82; +2.50° M = 95.10 %, SE = 2.03; $p < 0.001$). We also uncovered a significant interaction for which post-hoc pairwise t-tests run with a Bonferroni correction revealed key saccade amplitude effects at small forward shifts such as +0.25° (4° M = 86.26 %, SE = 2.46; 8° M = 71.83 %, SE = 3.84), t (29) = 4.76, $p < 0.05$, but no difference for large shifts (e.g., -2.50° and +2.50°, p = 1.0).

Table 1. Behavioral summary of ANOVA results for accuracy and reaction time across saccade amplitudes and target shifts.

Measure	Factor	*df*	*F*	*p*	η^2
Accuracy (%)	Saccade Amplitude	1, 29	37.42	< 0.001	0.02
	Target Shift	1.79, 52.04	10.74	< 0.001	0.19
	Interaction	3.69, 107.03	5.54	< 0.001	0.03
Reaction Time (%)	Saccade Amplitude	1, 29	5.68	< 0.05	0.01
	Target Shift	2.99, 86.62	22.64	< 0.001	0.18
	Interaction	5.89, 170.82	2.70	< 0.05	0.01

As to reaction time, a two-way analysis of variance (ANOVA) with repeated-measures and Greenhouse Geisser correction was performed to evaluate the effects of saccade amplitude (4° and

8°) and target shift (11 possible shifts) on reaction time. ANOVA results pertaining to reaction time are reported in Table 1. The ANOVA yielded a statistically significant main effect of saccade amplitude and was due to shorter reaction times following small saccade jumps (4° M = 81.40 %, SE = 2.91) relative to large saccade jumps (8° M = 84.63 %, SE = 2.84).

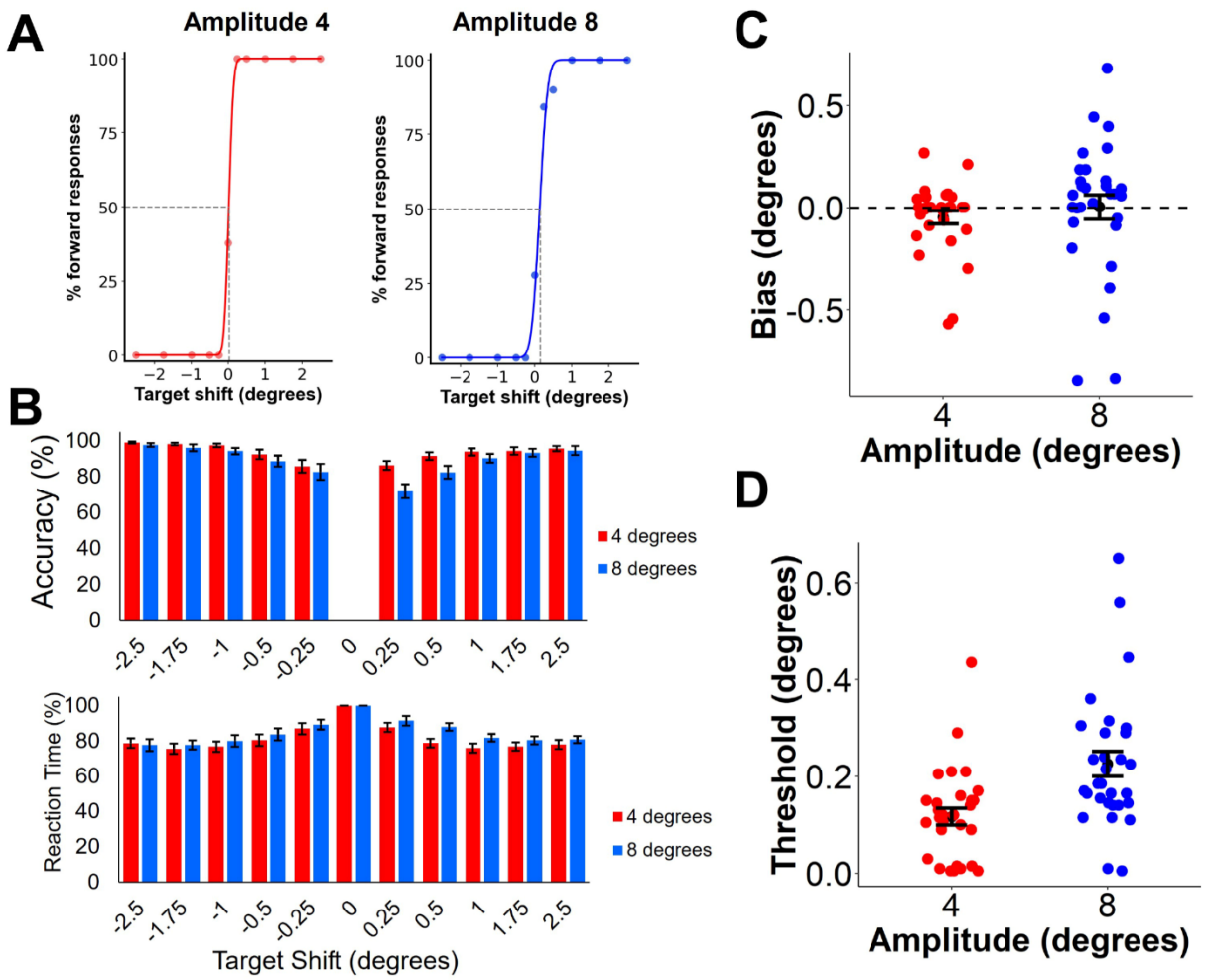

Fig 6. Behavioral and psychometric results across amplitude 4° and 8° trials.

(A) Psychometric curves (continuous line) fitted to the percentage of forward response data (individual filled circles) from a single subject across 4° (in red) and 8° trials (in blue). The bias is indicated with dashed lines and corresponds to the point on the psychometric curve with 50% forward responses. (B) Accuracy in participants' manual decision of the shift direction (encoded

as a percentage out of the total number of trials) and manual reaction time relative to each participant's reaction time at the 0 target shift across target shifts for the 4° (in red) and 8° trials (in blue). (C) Psychometric bias spread across the 4° (in red) and 8° trials (in blue). Individual subjects are indicated with colored filled circles, black filled circles represent the mean across subjects, and the black error bars represent the standard error of the means. (D) Psychometric threshold across the 4° (in red) and 8° trials (in blue). Individual subjects are indicated with colored circles, black filled circles represent the mean across subjects, and the black error bars represent the standard error of the means.

The ANOVA also uncovered a main effect of target shift mainly driven by progressively longer reaction times for short target shifts (e.g., -0.25° M = 88.13 %, SE = 2.98; +0.25° M = 89.53 %, SE = 2.64) relative to long target shifts (e.g., -2.50° M = 78.21 %, SE = 3.07; +2.50° M = 79.36 %, SE = 2.35; $p < 0.001$). Finally, there was a significant interaction across the saccade amplitude and target shift factors. Post-hoc pairwise t-tests run with a Bonferroni correction revealed key saccade amplitude effects at small forward shifts such as +0.50° (4° M = 78.79 %, SE = 2.45; 8° M = 88.01 %, SE = 2.17), t (29) = -4.59, $p < 0.05$, but no difference for large shifts (e.g., -2.50° and +2.50°, p = 1.0).

Saccadic Eye Movement Measures

In the experiment, we were interested in investigating the visual error the participants experienced on each trial. Fig 7 provides an illustration of an example participant's eye fixations following the initial saccade for the four possible target locations. There was a qualitatively larger spread around the initial targets that were further away from the fixation cross (and required an 8° saccade). We assessed potential gain proportion differences across saccade amplitudes with a two-

way repeated-measures ANOVA with Greenhouse Geisser correction. ANOVA results pertaining to gain are reported in Table 2. The ANOVA yielded a statistically significant main effect of gain type with a greater proportion of undershoots (*M* = 69.40 %, *SE* = 3.42) relative to overshoots (*M* = 30.60 %, *SE* = 3.42). There was also a significant interaction which indicated a greater proportion of undershoots for saccades of amplitude 8° (*M* = 75.38 %, *SE* =3.35) relative to trials with shorter saccades of amplitude 4° (*M* = 63.42 %, *SE* = 3.19; see Fig 7B).

Table 2. Perceptual summary of ANOVA results for gain across saccade amplitudes and gain types and for VE-shift congruency across saccade amplitudes and target shifts.

Measure	Factor	*df*	*F*	*p*	η^2
Gain	Saccade Amplitude	1, 29	0.00	1.00	< 0.01
	Gain Type	1, 29	37.62	< 0.001	0.55
	Interaction	1, 29	52.88	< 0.001	0.10
VE-shift congruency	Saccade Amplitude	1, 29	16.23	< 0.001	0.01
	Target Shift	2.91, 84.34	75.64	< 0.001	0.44
	Interaction	5.98, 173.44	12.84	< 0.001	0.04

We next assessed potential VE and target shift congruency differences across target shifts and saccade amplitudes. A two-way repeated-measures ANOVA with Greenhouse Geisser correction was run on VE-shift congruency. ANOVA results pertaining to gain are reported in Table 2. The ANOVA yielded a statistically significant main effect of saccade amplitude with more congruency across VE and target shift for shorter saccade jumps (4° *M* = 69.67 %, *SE* = 4.34) relative to longer saccade jumps (8° *M* = 65.30 %, *SE* = 5.08). The ANOVA also revealed a main effect of target shift which was driven by more incongruent VEs for short backward target shifts (e.g., -0.25° *M* = 36.67 %, *SE* = 3.87) relative to large target shifts (+2.50° *M* = 86.33 %, *SE* = 3.26, *p* < .001; -2.50°

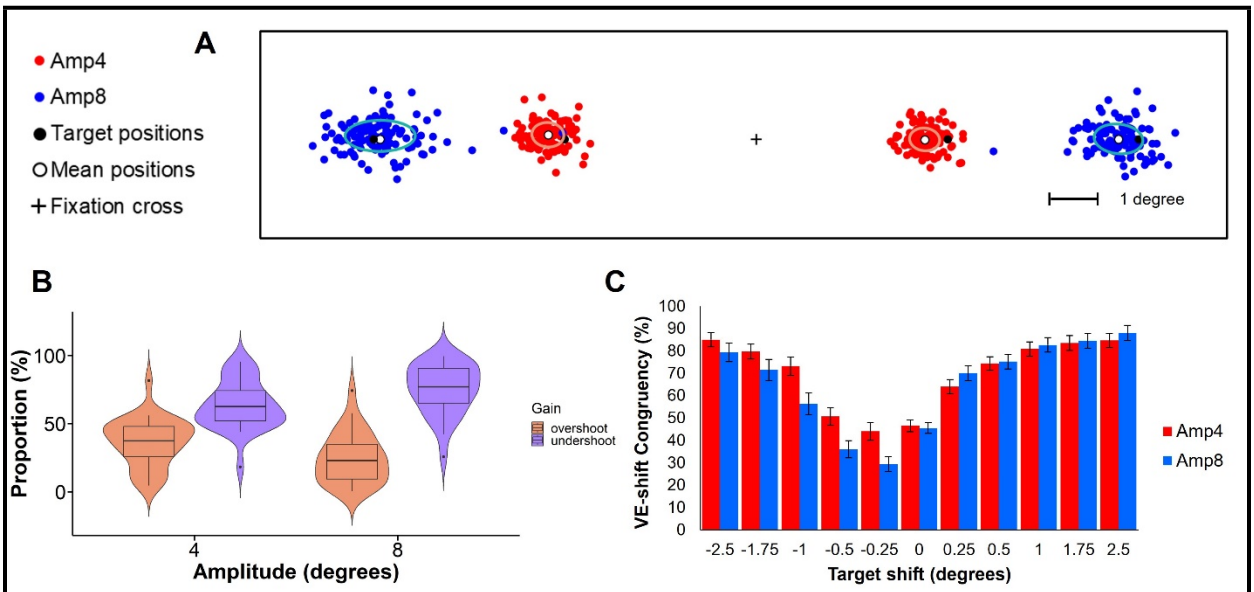

Fig 7. Illustration of eye fixations, gain, and shift-VE congruency across trials with saccade jumps of 4° and 8°.

(A) Example of eye fixations after the initial saccade across trials in an individual participant. Red filled circles correspond to individual trials requiring a 4° saccade to the left or right of the fixation cross. Blue filled circles correspond to individual trials requiring a 8° saccade to the left or right of the fixation cross. Black filled circles indicate the target positions (left/right and 4°/8°). White circles indicate the mean positions within the corresponding eye fixation clusters. Colored ellipses indicate the spread around the mean positions in terms of 1 standard deviation of a normal Gaussian. (B) Proportions of trials with overshoots and undershoots computed in terms of the gain relative to initial target position. Gain was calculated separately across 4° and 8° trials. Distributions of gains are shown with a violin plot and box plot. Brown distributions correspond to overshoots. Purple distributions correspond to undershoots. (C) VE-shift sign congruency across trials involving saccade jumps of amplitude 4° (in red) and 8° (in blue).

585

M = 82.17 %, *SE* = 3.76, *p* < .001). Finally, a significant interaction revealed that trials involving small backwards target shifts yielded lower levels of VE-shift congruency following larger saccade jumps of 8° (-0.25° *M* = 29.33 %, *SE* = 3.23) relative to 4° saccades (-0.25° *M* = 44.00 %, *SE* = 4.04), but there were no VE-shift congruency differences across saccade amplitudes for large forward shifts (*p* = 1.0; see Fig 7C).

Predictive Effects of Visual Error on Accuracy

Fig 8 presents a characterization of the VEs and their ability to predict response accuracy across backward and forward target shifts. We first fit the proportions of backward vs. forward VEs across target shifts with a logistic function (see equation 3). The fitted logistic curve had an imposed [-1,1] range and an inflection point x_0 with 0 as its y-coordinate. Panel 8A displays the group logistic fit averaged from trials with saccade jumps of 4° and 8°. The bias is shown with a red arrow to indicate the lateral shift of the logistic function along the target shift degree direction relative to a theoretical VE step function. This function reflects an immediate corresponding shift from backward VEs to forward VEs at the middle 0° target shift point. At the group level, the inflection point reflected a VE bias shift of -0.48° (*SE* = 0.08), with a greater negative VE bias at trials with larger saccade jumps (8° *M* = -0.71°, *SE* = 0.12) relative to trials involving smaller saccade jumps (4° *M* = -0.24°, *SE* = 0.05), *t* (29) = 5.89, *p* < 0.001. This result is further reflective of the greater proportion of undershoots following larger saccade amplitudes and lower VE-shift congruency for small backward target shifts (see Fig 7C).

At the individual level, one can investigate the VE profile across target shifts, and the VEs' corresponding relationship with response accuracy. In the case of the example subject shown in Fig 8B, the VE bias shift based on the logistic function fit is estimated as -1.26° (4° VE bias = -

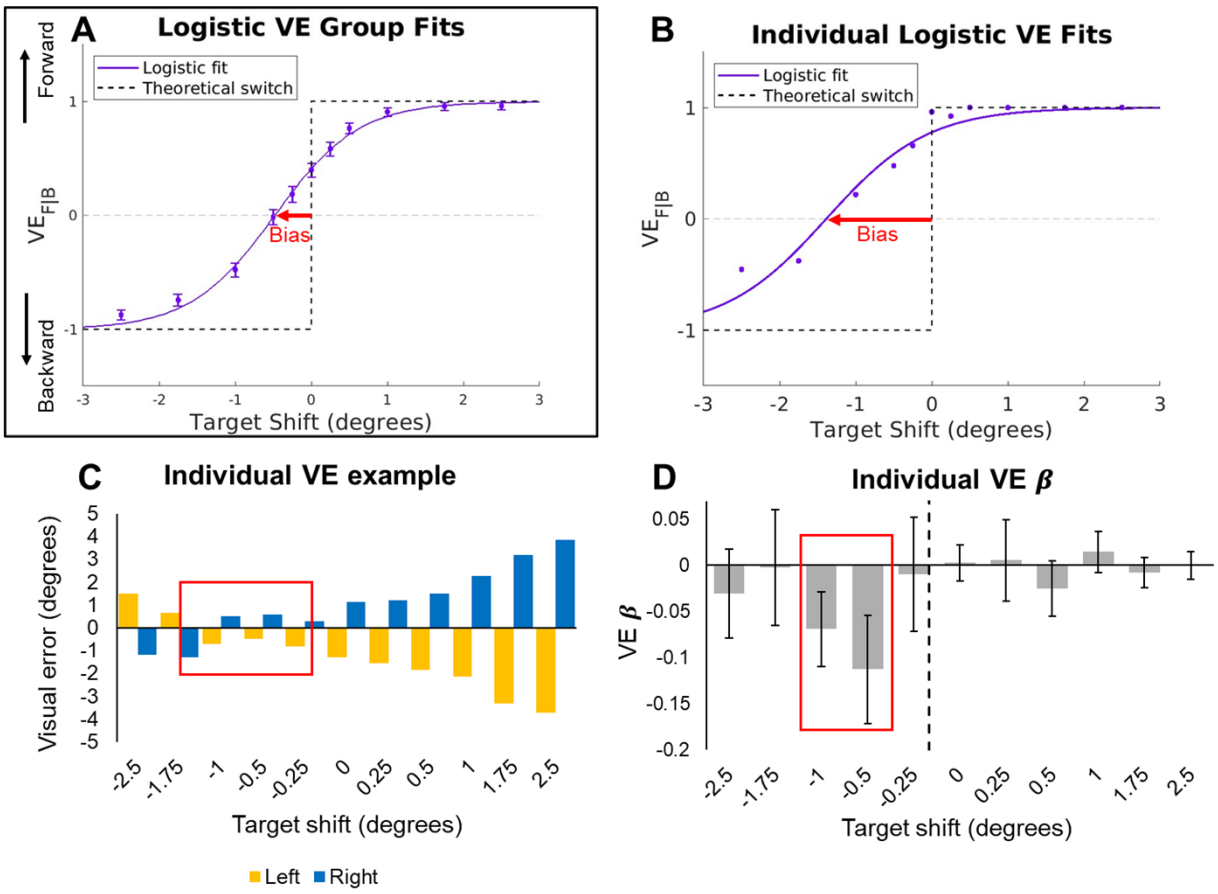

Fig 8. VE characterization and VE β distribution example across backward and forward target shifts.

(A) Proportions of forward vs. backward VEs across target shifts, fitted at the group level with a logistic function across 4° and 8° saccade jumps and averaged, as shown with a purple line. Individual filled circles correspond to group $VE_{F|B}$ mean proportions for each target shift, along with their SEM, as shown with error bars, reflecting variability across individuals. The logistic function is fit with a fixed [-1,1] range where -1 reflects 100 % backward VEs at that target shift, and +1 reflects 100 % forward VEs at that target shift. A dashed line indicates the theoretical shift from backward to forward VEs with a step function. (B) Individual logistic fit of the $VE_{F|B}$ proportions for an example subject. Individual filled circles correspond to the subject $VE_{F|B}$ means at each target shift. (C) Signed VE illustration across trials involving leftward and rightward saccades across target shifts. For the same example subject, VEs corresponding to trials with leftward saccades are shown with yellow bars, and VEs

0.69°; 8° VE bias = -1.82°). This bias is further reflected in panel 8C (see red box). Specifically, we see that for the backward target shifts -1.00°, -0.50°, and -0.25°, there is an early reversal of the VE sign across trials involving leftward vs. rightward saccades. Such reversal is also captured by mixed proportions of forward and backward VEs as shown in panel 8B. Note that both at the group and individual levels, it is possible to express the forward/backward proportion quantity in terms of VE-based estimates of the target location in the form of a psychometric function as was done previously by Bansal et al. [45] (see Fig S2 for corresponding logistic fits, Fig S3 for psychometric functions broken down across saccade amplitude and direction at the group level, and see Fig S4 for psychometric functions broken across saccade amplitude and direction at the individual level).

By further inputting the signed VEs in a linear model to predict the corresponding response accuracy, encoded as a binary measure (0 vs. 1), we can estimate the predictive ability of the VEs to capture participants' resulting perceptual judgments in the form of a β coefficient. In the case of this example subject, the signed VEs were most reflective of response accuracy at target shifts -1.00°, -0.50°. Mathematically, this effect is due to a *greater consistency* in the VE signs across trials with leftward vs. rightward saccades, which would be expected to cancel each other out due to opposite VE sign encodings, as is the case for large forward target shifts (see Fig 1 and Fig 8C). Therefore, target shifts for which the signed VEs better predict response accuracy indicate cases in which the VE-shift incongruency (as shown with backward target shifts in Fig 7C) meaningfully gets translated into impaired perceptual judgments and can be directly represented as the *absolute value* of the VE β coefficient. One can subsequently compute the *lateral bias,* which is the center of gravity of the |VE β| vector across target shifts, and represent the perceptual biasing effect of

the VEs on *response accuracy* (see Methods for more details on the computation of the lateral bias).

Lateral Bias and RT Estimation from VE β

Fig 9 presents a snapshot of individual variability across VE βs and lateral biases, as well as inter-individual bias correlation with accuracy. While most participants tended to have a negative lateral bias (M = -0.06°, SE = 0.02°) such as Participant B (weigh. bias = -0.17° shown with purple symbols), a few other participants such as participant C had a positive lateral bias (weigh. bias = 0.09° shown with green symbols) and yet others were close to not having any biases at all (weigh. bias = -0.02° shown with orange symbols). At the group level, we found that participants with a lateral bias closer to 0° also tended to have higher response accuracy in the visual perception task, r (28) = 0.64, $p < 0.001$ (see Fig 9). In addition, the lateral bias based on the vector of |VE β| was

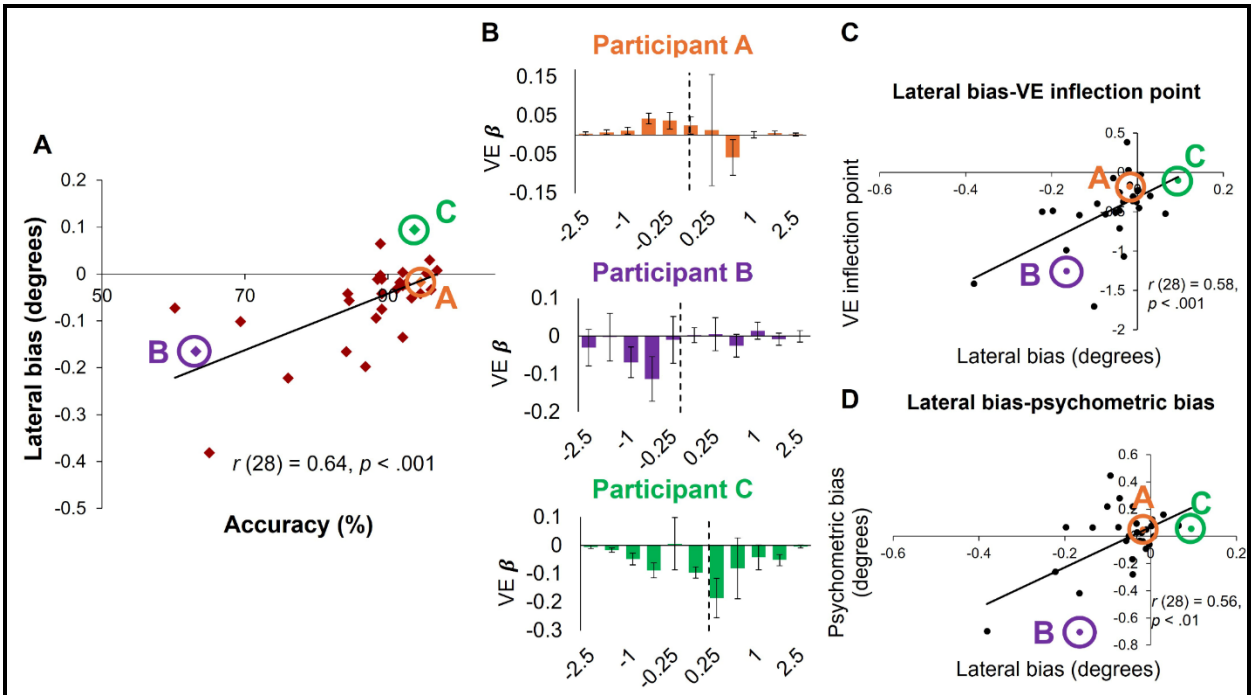

Fig 9. Lateral bias and relationship with accuracy and psychometric bias across participants.

(A) Scatter plot showing the correlation between the lateral bias and accuracy. Three example participants are labeled with the letters 'A', 'B', and 'C'. (B) Distribution of VE β coefficients across target shifts in the three representative participants 'A', 'B', and 'C'. Participant A corresponds to an example with no major lateral bias. Participant B corresponds to an example with a negative lateral bias. Participant C corresponds to an example with a positive lateral bias. A dashed black line indicates each participant's lateral bias. (C) Scatter plot showcasing correlation between the lateral bias and the VE-based inflection point with the three characteristic participants. (D) Scatter plot showcasing correlation between the lateral bias and the psychometric bias with the three characteristic participants.

found to be positively correlated with the $VE_{F|B}$ inflection point x_0, r (28) = 0.58, $p < 0.001$, and with the psychometric bias, r (28) = 0.56, $p < 0.01$ (see Fig 9). Overall, this suggests that this

measure is both reflective of perceptual information and perceptual judgment biases across target shifts.

To explicitly relate the VE β individual vectors to decision-making, we leveraged the DDM framework to fit individuals' varying reaction time profiles across target shifts (see Fig 3). In order to mechanistically tie the VE coefficients to decision-making model parameters, we designed two separate versions which either included or did not include a decision-making bias parameter. The version of the model with no bias corresponded to a perfectly symmetric model in which trial RTs resulting from judgments following backward target shifts always matched the trial RTs resulting from judgments following forward target shifts (see Fig 5a). Such a model exactly estimated three DDM parameters: *drift rate*, *decision bound*, and the *non-decision time*. On the other hand, the alternative version of the DDM had an additional bias parameter which shifted the starting point by a fixed offset (see Fig 5b) thus resulting in an asymmetry across RTs resulting from forward target shifts vs. backward target shifts. Therefore, this alternative version of the DDM estimated four parameters. For each model, two separate sets of parameters were estimated for each saccade amplitude (4° and 8°).

To assess any meaningful relationship between the DDM biasing parameter and the VE β coefficients, we used a linear mixed-effects model (LMEM) to explaining RT based on VE β across all trials from all subjects while taking into account random intercepts corresponding to each participant ($N = 30$), each saccade amplitude (4° and 8°), and each target shift (11 possible target shift, see Fig 2 and Fig 4). LMEM analyses did not yield any significant effect of VE β on RT in the uniform DDM with no bias (VE_β $\gamma = 42.51$, $p = 0.15$; CI = [-15.50, 100.52]). However, LMEM analyses revealed a significant effect of VE β on RT in the DDM with an additional decision-making biasing parameter (VE_β $\gamma = 174.03$, $p = 0.15$; CI = [80.09, 267.96]). These

results demonstrate that VEs' accuracy weights are suitable to mechanistically account for decision-making biases as part of the DDM framework.

DDM Individual Fits of Choice Data and Reaction Time

The next step was to leverage the vector of VE βs for each subject to simulate the effects of a participant's bias on their decision-making process in the visual perception task. This vector was appended to the matrix of inputs in the DDM along with choice (% forward responses) and manual reaction time data. To reiterate, the VE βs were used to bias the drift rate as illustrated in Fig 5C such that the drift rate offset would be directly proportional to the corresponding target shift's VE β. In the DDM, this in turn altered the reaction time at that target shift. The final hybrid DDM still included an estimated DDM bias to shift the starting point for evidence accumulation, but the addition of the VE β into the model provided *explanatory* evidence to estimate the extent to which VE-related information biased the decision-making process.

The new DDM with the incorporation of the vector of VE βs was simultaneously fit to participants' choice data and reaction time data as illustrated on Fig 4. For each participant and each saccade amplitude, the model estimated 5 parameters: drift rate, decision bound, bias, non-decision time, and a final *weight* parameter which scaled the effect of the corresponding VE β coefficients across target shifts to estimate the best drift rate offset as a measure of decision-making VE-based bias. Similar to the previous DDM simulations, two separate sets of such parameters were estimated for each saccade amplitude (4° and 8°).

Based on the best fit resulting from the likelihood method, the model simulated the psychometric curve and reaction time profile that matched the best-fit parameters. Psychometric simulated choice data were compared against experimental data with the BIC to assess the appropriateness of the DDM model fit. Such BIC was compared to the beta binomial best-fit

estimates as described earlier. There was no statistically significant difference in BIC between the psychometric manual choice fits and the DDM manual choice fits, t (29) = 0.66, p = 0.51, (DDM M = -48.77, SE = 2.70; Psychometric M = -50.22, SE = 3.06). Therefore, the DDM successfully simulated choice data at a similar level as the beta binomial model. In terms of reaction time, we found that the DDM with a bias captured the RT data to a greater extent (4° R^2 = 0.46; 8° R^2 = 0.50) relative to the DDM that did not include any bias (4° R^2 = 0.36; 8° R^2 = 0.30).

In addition to capturing participants' choice data, the DDM fit reaction time data and leveraged the incorporation of the vector of VE βs to estimate drift rate offsets to simulate VE-based decision making biases over the course of evidence accumulation. Fig 10 provides detailed results for the three representative participants A, B, and C, and presents their corresponding psychometric and reaction time profiles along with their DDM model fits. As a reference, we also depicted a uniform version of the DDM that assumed symmetry across forward and backward target shifts.

Specifically, participant A had a VE β, or lateral bias, close to 0°. Their psychometric curves display point symmetry across the forward and backward trials while their manual reaction time profiles display reflection symmetry across forward and backward trials. Furthermore, this symmetric relationship is also reflected by the significant overlap between the psychometric and reaction time profiles across the two types of DDM simulations, with and without a bias term. Participant A's high accuracy levels (see Fig 9) are reflected in their psychometric curves which resemble step functions; a very small shift in the target was required for accurate shift direction detection (i.e., a small threshold). In terms of reaction times, we found that the 0 target shift had the slowest reaction times, and this time tended to decrease (i.e., react faster) in both the forward and backward direction as the target shift increased in magnitude. Participant A's DDM-based VE

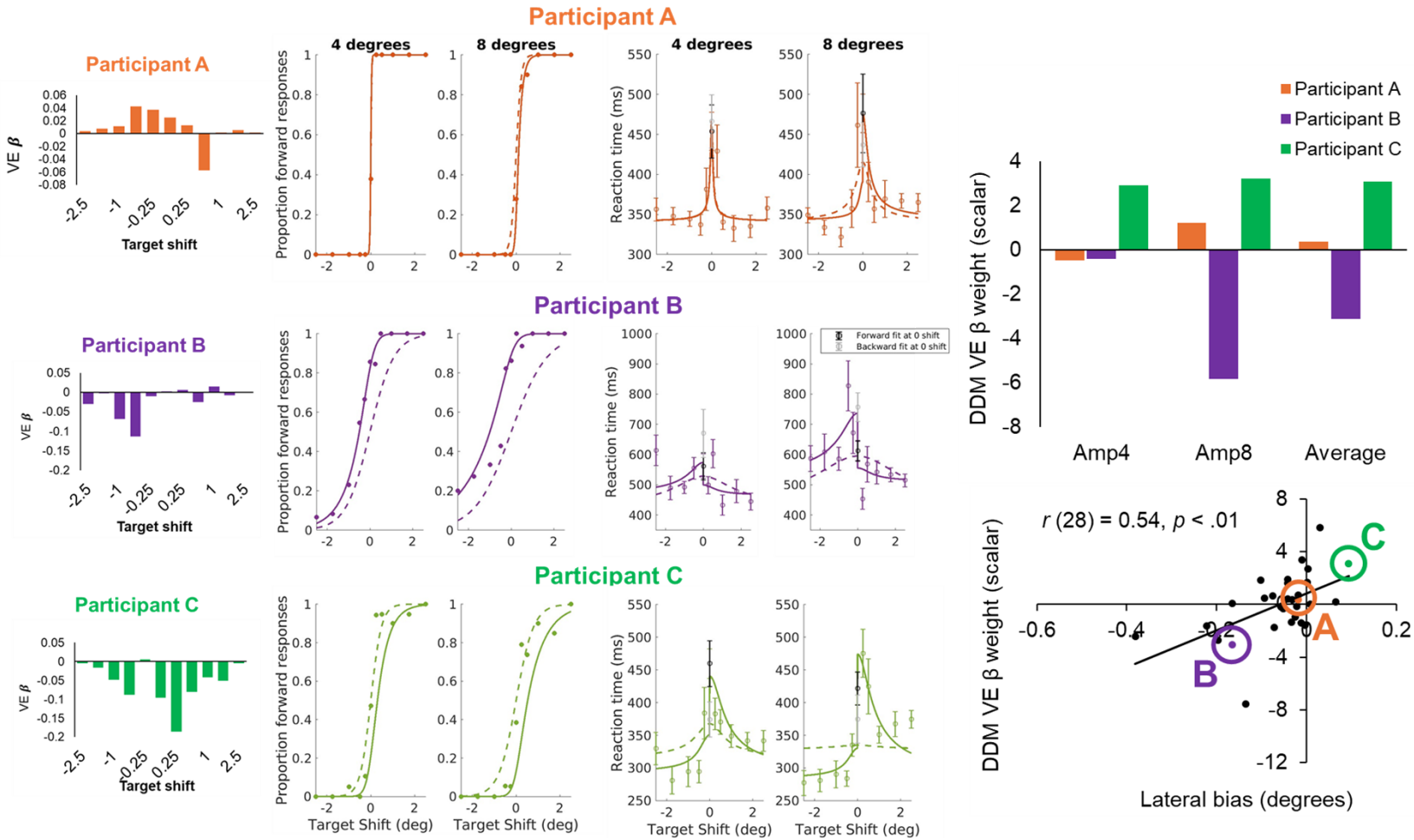

Fig 10. Psychometric and reaction time curve fits based on DDM simulations and illustration of lateral bias' effect on model fits.

Three participants' psychometric and reaction time curves were fitted to the data broken down by target shift based on DDM simulations across 4° and 8° trials. Manual reaction time data differentiate between forward (in black) and backward reaction times (in gray) at the 0 target shift. Dashed lines correspond to DDM simulations with the baseline model assuming decision-making symmetry across backward and forward target shifts. Solid lines correspond to DDM simulations from the model that incorporates a bias term and a VE-based weight. For reaction time data, circles indicate the mean, and the error bars indicate the standard error of the means. An illustration of the spread of each participant's lateralization biases is provided to the left of the graph. Participant A corresponds to an example of a lateral bias being close to 0 and is shown in orange at the top. Participant B corresponds to an example of a negative lateral bias and is shown in purple in the middle. Participant C corresponds to an example of a positive lateral bias and is shown in green at the bottom. On the right, individual DDM-based VE β weights are shown for each of the three participants across the two saccade amplitudes, and as an average across both types of simulations. At the bottom, a cluster plot shows the positive correlation between the lateral bias and the DDM-based VE β weights.

β weight was estimated as a scalar with a small magnitude and was inconsistent across trials with saccade amplitudes 4° and 8°, reflecting little to no contribution of the VE to decision-making.

Participant B was characterized by a negative lateral bias. Their psychometric curves display greater proportions of forward responses for backward target shifts indicating erroneous decisions along the backward direction. Specifically, the negative lateral bias was particularly salient when comparing the psychometric model fits with a DDM bias term relative to the psychometric model fits with no bias term. The main result is that the DDM bias term is necessary to account for a backward shift of the psychometric curve, and is well accounted for by the vector of VE βs. In terms of manual reaction time, we found that the participants' data fit better with an asymmetric version of the DDM with slower reaction times along the backward direction relative to forward target shifts. Participant B's DDM-based VE β weight was estimated as a scalar with a large magnitude and was consistently negative across trials with saccade amplitudes 4° and 8°, reflecting the negative VE bias contribution to decision-making.

Lastly, participant C was characterized by a positive lateral bias. Their psychometric curves display greater proportions of backward responses for forward target shifts indicating erroneous decisions along the forward direction. Specifically, the positive lateral bias was particularly salient when comparing the psychometric model fits with a DDM bias term relative to the psychometric model fits with no bias term. The main result here is that the DDM bias term is necessary to account for a forward shift of the psychometric curve, and is also well accounted for by the vector of VE βs. In terms of manual reaction time, we found that the participant's data was better represented by an asymmetric version of the DDM with slower reaction times along the forward direction relative to backward target shifts. Participant C's DDM-based VE β weight was estimated as a scalar with a medium magnitude and was consistently positive across trials with saccade

amplitudes 4° and 8°, reflecting the positive VE bias contribution to decision-making (Note that all individual participants' psychometric curves and reaction time profiles can be found in the linked repository).

At the group level, we found that the DDM VE β weight was positively correlated with the lateral bias, r (28) = 0.54, $p < 0.01$. This result indicates that the participants that tended to have a greater VE-based bias (i.e., more pronounced shift of the center of gravity away from no bias – that is, 0°) also had a greater DDM VE β weight reflecting a larger contribution of such β coefficients towards the drift rate offset. In addition, inputting negative lateral biases in the DDM tended to yield negative DDM VE β weights, whereas inputting positive lateral biases in the DDM tended to yield positive DDM VE β weights. The reason for this is that the drift rate was proportional to the target shift input, which is defined as $input = s + w \times \beta_s$, where s indicates any given shift, β_s denotes the corresponding VE β, and w refers to the DDM VE β weight (see Fig 5C). Overall, the lateral bias and the DDM VE β weight jointly accounted for the degree of bias in evidence accumulation throughout the decision-making process.

Discussion

In this study, we leveraged the DDM framework to characterize the evidence accumulation process that underlies the perception of visual stability across saccadic eye movements. One key new feature was the incorporation of the visual error (VE) to account for the visuospatial biasing effects of sensory processing on decision making. We adapted a trans-saccadic shift detection task from previous research [45,51] and examined participants' decision-making behavior throughout the task. We measured perceptual sensitivity in terms of the psychometric bias and the psychometric threshold, and we operationalized decision-making behavior in terms of reaction

time and response accuracy. We expected small target shifts to induce a greater bias in terms of decision-making as would be predicted from the saccadic suppression of displacement (SSD). Computationally, we focused on the hypothesis that by incorporating the visual error the DDM would capture subsequent perceptually-based biases on decision-making and perception.

Psychometric & Perceptual Profiles

We found that participants' psychometric profiles were consistent with previous findings [21,24,25,51]. The psychometric threshold increased proportionally to the initial saccade's amplitude (Fig 6), which suggests that small target shifts were more difficult to detect after larger saccades. In addition, smaller target shifts were associated with lower decision accuracy and slower reaction times, as would have been expected based on previous findings (Fig 6)[42]. This result is aligned with the main assumptions of the DDM, which posits that an increase in the target shift magnitude should be associated with a monotonic increase in accuracy and decrease in reaction time [43].

We also found that participants tended to undershoot the target after the initial saccade, which aligns with previous experimental reports of participants falling short of the intended visual targets (Fig 7) [40,41,45]. In this study, this resulted in greater incongruency between the direction of the target shift and the visual error across trials involving small backward target shifts. Subsequently, when explicitly computing the proportion of backward vs. forward visual errors, we found a negative group-level perceptual bias characterized by greater proportions of forward VEs for small backward shifts. Because of the SSD, it could be the case that small target shifts directly following the saccade also impacted perceptual sensitivity, particularly around the eye endpoint location. Since participants had a propensity to undershoot the visual target, such endpoint locations tended to occur in the backward direction (Fig 6 and Fig 7). In cases in which one might expect such

undershoots to play a significant role in biasing decision-making, we would in turn expect that participants' psychometric functions would align with predictions solely derived from the VE, as was previously reported in patients with psychosis (Fig 7) [25,45,51].

To combine the perceptual and behavioral dimensions, we computed coefficients related to the VEs that estimated participants' manual choice accuracy. Such coefficients were particularly sensitive to VEs' sign encodings resulting from leftward and rightward saccades. The main result was that target shifts that involved more consistent signed VEs, with smaller magnitude, tended to result in more significant VE βs. These coefficients are meaningful in so far as they provide a way to identify the specific target shifts at which incongruencies in visual errors across trials with leftward and rightward saccades tended to significantly predict shift direction choice accuracy (Fig 8). Furthermore, one can compute a lateral bias defined as the center of gravity of the VE-based coefficients to determine the extent to which VEs impacted manual choice accuracy.

At the group level, the lateral bias was found to explain participants' general accuracy levels in the trans-saccadic task (Fig 9). At the perceptual level, the bias was found to be significantly correlated with VE proportions' inflection bias, which indicates the extent to which perception was biased along the backward or forward direction. At the behavioral level, the bias was found to be significantly correlated with the psychometric bias which indicates the extent to which perceptual judgments' sensitivity was shifted (i.e., biased) in the forward or backward direction. Therefore, since the lateral bias is derived from participants' distribution of VE β coefficients, it constitutes a summary measure that captures relevant information pertaining to both perceptual and psychometric dimensions.

DDM Framework & Perceptual Bias on Decision-Making

With regards to computational modeling, we found that the DDM could explain manual choice and reaction times based on an evidence accumulation process that resulted in perceptual decisions. We first compared two different versions of the DDM: The first one corresponded to a fully symmetric uniform version of the model in which the decision time for backward target shifts precisely matched the decision time for trials with forward target shifts of the same magnitude. The second one corresponded to an asymmetric version of the model in which the starting point was offset by a fixed bias. Based on a linear mixed-effects model, we determined that reaction time could only be estimated by the VE β coefficients from the linear modeling technique in the latter version of the DDM that incorporated a bias term. Therefore, we concluded that such coefficients could be used as the basis for modeling perceptually-based decision making biases.

When incorporating the VE-based coefficients into the DDM, we found that we could capture individual positive and negative biases in contrast to the uniform version of the DDM (Fig 10). In addition, we showed that the VE-based DDM could simulate individuals' decision-making biases based on a range of idiosyncratic DR offsets corresponding to each target shift. Therefore, this hybrid version of the DDM provides a more granular representation of individuals' perceptually-based decision-making biases relative to single psychometric bias estimates. Furthermore, it provides an additional explanatory step since the framework can tie specific decision-making biases to perceptual properties related to the VE.

One novel feature of the hybrid version of the DDM is the estimation of a special *weight* parameter that scales the effect of the corresponding VE β coefficients on the drift rate offset across all target shifts. Such DDM VE β weight was estimated along with the DR, bias, non-decision time, and decision bound for each set of trials involving small (4°) or large (8°) saccades. The magnitude of this weight parameter is significant in so far as it determines the extent to which the

VE-based coefficients should bias the DR offset at particular target shifts. Inter-individual investigation of this weight across saccade types revealed a positive correlation with the lateral bias (Fig 10). Future research may leverage the properties of the DDM VE-based weight to design novel biomarkers that could be the basis for neural investigations of decision-making biases in patient populations.

From a mechanistic perspective, one can think of the visual error as a teaching signal that drives internal model computations and estimations [11,52–55]. Other computational models of internal models and corollary discharges, (e.g., Masselink and Lappe, 2021 [56]), implemented an error backpropagation mechanism akin to the delta rule to progressively optimize saccadic eye movements. Simulation results from such analyses suggest that visuomotor learning may likely be driven by a postdictive motor error instead of the visual prediction error. However, such models often do not make explicit assumptions about how the decision-making process pertaining to perceptual judgments may be altered over time. One avenue for future research would be to develop a hybrid framework that would be capable of simulating progressively more refined eye movements based on postdictive motor error signals, and generate explicit behavioral perceptual judgment predictions.

Relevance of Findings for Clinical Applications

How can this framework be useful beyond the study of healthy control participants? Previous research has found that certain patient populations (e.g., patients experiencing psychotic symptoms, e.g., Schizophrenia) are characterized by abnormalities in perceptual organization and deficits in bottom-up processing [57–60], which may lead to impaired perceptual judgments. Behaviorally, it was found that responses from patients experiencing psychosis were more consistent with VE-based responses whereas responses from healthy controls were more consistent

with estimated responses from a mixture of externally-based and internally-based signals [45]. Computational models such as the DDM introduced here provide a useful framework for quantifying the degree to which behavior is impacted by an over-reliance on bottom-up sensory cues relative to internally generated signals. In addition, numerous studies have postulated neural mechanisms that may support DDM-like decision processes [23,28,29,61–64].

In terms of neural mechanisms linking to our results, previous research has found that the saccadic eye-movement corollary discharge actively contributes to anticipatory visual sensitivity at the level of the frontal eye field (FEF, Brodmann Area 8) [52,65]. Specifically, inactivation of the collicular-thalamic-cortical neural pathway involving the superior colliculus, medio-dorsal thalamic nucleus, and the FEF, led to impairments of behavior reliant on internal monitoring of the saccadic eye-movement [65–67]. However, other neural systems likely play a role as well such as the basal ganglia [68], the paramedian pontine reticular formation in the brain stem [69], and the vermis and fastigial oculomotor region in the cerebellum [70]. Assuming that the internally-generated signals are inherently linked to predictive mechanisms, an impairment in the brain's ability to predict the sensory consequences of motor commands would lead to motor errors and disturbances in one's sense of agency. Moberget and Ivry (2019) [71] suggested that many cognitive and sensorimotor symptoms experienced by individuals with psychosis may in part be due to dysfunction in cerebellar circuitry. Such dysfunction could also contribute to higher-level cognitive deficits resulting in working memory impairments and thought disorder. One potential neural pathway that would mediate such dysfunction is the cerebello-thalamo-cortical pathway, which alongside DLPFC and PPC deficits could underlie DR impairments associated with decision-making [43,44,71,72]. A comparison of behavioral biasing effects and cerebello-cortical

connectivity could help shed light on the involvement of the cerebellum in psychosis and internal model-related predictive mechanisms.

In sum, the present study augmented the DDM framework with the novel addition of visual error information to computationally describe the behavioral asymmetric biases over the course of evidence accumulation. We found that the lateral bias based on a distribution of VE-based lateralization weights provided further insight into the asymmetric behavioral patterns previously accounted for by the psychometric bias. Such weights could also account for negative and positive biasing effects on reaction time and error rates. Furthermore, the DDM DR coefficient and DDM bias parameters provided mechanistic insight into the speed and accuracy of perceptual decisions, and helped capture behavioral asymmetric patterns. Future research will investigate the utility of an augmented DDM in clinical contexts, for instance involving patients experiencing psychosis, to shed light on the precise neural circuitry involved in perceptually-based computations and sensorimotor learning.

Acknowledgments

We would like to thank Grace Shen and Staci Board for help with data collection.

References

1. Wurtz RH. Neuronal mechanisms of visual stability. Vision Research. 2008;48: 2070–2089. doi:10.1016/j.visres.2008.03.021

2. Higgins E, Rayner K. Transsaccadic processing: stability, integration, and the potential role of remapping. Atten Percept Psychophys. 2015;77: 3–27. doi:10.3758/s13414-014-0751-y

3. Wurtz RH, Joiner WM, Berman RA. Neuronal mechanisms for visual stability: progress and problems. Phil Trans R Soc B. 2011;366: 492–503. doi:10.1098/rstb.2010.0186

4. Feinberg I. Efference Copy and Corollary Discharge: Implications for Thinking and Its Disorders. Schizophrenia Bulletin. 1978;4: 636–640. doi:10.1093/schbul/4.4.636

5. Hauser M, Moore JW, de Millas W, Gallinat J, Heinz A, Haggard P, et al. Sense of agency is altered in patients with a putative psychotic prodrome. Schizophrenia Research. 2011;126: 20–27. doi:10.1016/j.schres.2010.10.031

6. Frith CD. The Cognitive Neuropsychology of Schizophrenia (Classic Edition). New York, NY: Psychology Press and Routledge Classic Editions.; 2015.

7. Ondobaka S, De Lange FP, Wittmann M, Frith CD, Bekkering H. Interplay Between Conceptual Expectations and Movement Predictions Underlies Action Understanding. Cereb Cortex. 2015;25: 2566–2573. doi:10.1093/cercor/bhu056

8. Wolpert DM, Miall RC, Kawato M. Internal models in the cerebellum. Trends in cognitive sciences. 1998;2: 338–347.

9. Kawato M. Internal models for motor control and trajectory planning. Current Opinion in Neurobiology. 1999;9: 718–727. doi:10.1016/S0959-4388(99)00028-8

10. Kawato M, Ohmae S, Hoang H, Sanger T. 50 Years Since the Marr , Ito , and Albus Models of the Cerebellum. Neuroscience. 2021;462: 151–174. doi:10.1016/j.neuroscience.2020.06.019

11. Joiner WM, Fitzgibbon EJ, Wurtz RH. Amplitudes and directions of individual saccades can be adjusted by corollary discharge. J Vis. 2010;10: 22.1–12. doi:10.1167/10.2.22

12. Takano S, Matsumiya K, Tseng C, Kuriki I, Deubel H, Shioiri S. Displacement detection is suppressed by the post-saccadic stimulus. Sci Rep. 2020;10: 9273. doi:10.1038/s41598-020-66216-1

13. Bridgeman B, Hendry D, Stark L. Failure to detect displacement of the visual world during saccadic eye movements. Vision Research. 1975;15: 719–722. doi:10.1016/0042-6989(75)90290-4

14. Westheimer G. Sensitivity for vertical retinal image differences. Nature. 1984;307: 632–634. doi:10.1038/307632a0

15. Gysen V, Graef PD, Verfaillie K. Detection of intrasaccadic displacements and depth rotations of moving objects q,qq. Vision Research. 2002.

16. Niemeier M, Crawford JD, Tweed DB. Optimal transsaccadic integration explains distorted spatial perception. Nature. 2003;422: 76–80. doi:10.1038/nature01439

17. Atsma J, Maij F, Koppen M, Irwin DE, Medendorp WP. Causal Inference for Spatial Constancy across Saccades. Beierholm U, editor. PLoS Comput Biol. 2016;12: e1004766. doi:10.1371/journal.pcbi.1004766

18. Stewart EEM, Valsecchi M, Schütz AC. A review of interactions between peripheral and foveal vision. Journal of Vision. 2020;20: 2. doi:10.1167/jov.20.12.2

19. Deubel H, Schneider WX, Bridgeman B. Postsaccadic target blanking prevents saccadic suppression of image displacement. Vision Research. 1996;36: 985–996. doi:10.1016/0042-6989(95)00203-0

20. Deubel H, Bridgeman B, Schneider WX. Immediate post-saccadic information mediates space constancy. Vision Research. 1998;38: 3147–3159. doi:10.1016/S0042-6989(98)00048-0

21. Bansal S, Jayet Bray LC, Peterson MS, Joiner WM. The effect of saccade metrics on the corollary discharge contribution to perceived eye location. Journal of Neurophysiology. 2015;113: 3312–3322. doi:10.1152/jn.00771.2014

22. Green, David M. S John A. Signal Detection Theory and Psychophysics. The Quarterly Review of Biology. 1967;42: 578–578. doi:10.1086/405615

23. Cerracchio E, Miletić S, Forstmann BU. Modelling decision-making biases. Front Comput Neurosci. 2023;17: 1222924. doi:10.3389/fncom.2023.1222924

24. Joiner WM, Cavanaugh J, FitzGibbon EJ, Wurtz RH. Corollary discharge contributes to perceived eye location in monkeys. Journal of Neurophysiology. 2013;110: 2402–2413. doi:10.1152/jn.00362.2013

25. Jayet Bray LC, Bansal S, Joiner WM. Quantifying the spatial extent of the corollary discharge benefit to transsaccadic visual perception. Journal of Neurophysiology. 2016;115: 1132–1145. doi:10.1152/jn.00657.2015

26. Ratcliff R, Smith PL. A Comparison of Sequential Sampling Models for Two-Choice Reaction Time. Psychological Review. 2004;111: 333–367. doi:10.1037/0033-295X.111.2.333

27. Ratcliff R, McKoon G. The Diffusion Decision Model: Theory and Data for Two-Choice Decision Tasks. Neural Computation. 2008;20: 873–922. doi:10.1162/neco.2008.12-06-420

28. Mulder MJ, Van Maanen L, Forstmann BU. Perceptual decision neurosciences – A model-based review. Neuroscience. 2014;277: 872–884. doi:10.1016/j.neuroscience.2014.07.031

29. Forstmann BU, Turner BM, editors. An Introduction to Model-Based Cognitive Neuroscience. Cham: Springer International Publishing; 2024. doi:10.1007/978-3-031-45271-0

30. Gold JI, Shadlen MN. The Neural Basis of Decision Making. Annual Review of Neuroscience. 2007;30: 535–574. doi:10.1146/annurev.neuro.29.051605.113038

31. Ratcliff R. A theory of memory retrieval. Psychological Review. 1978;85: 59–108. doi:10.1037/0033-295X.85.2.59

32. Anders R, Riès S, van Maanen L, Alario F-X. Evidence accumulation as a model for lexical selection. Cognitive Psychology. 2015;82: 57–73. doi:10.1016/j.cogpsych.2015.07.002

33. Krajbich I, Hare T, Bartling B, Morishima Y, Fehr E. A Common Mechanism Underlying Food Choice and Social Decisions. PLOS Computational Biology. 2015;11: e1004371. doi:10.1371/journal.pcbi.1004371

34. Basten U, Biele G, Heekeren HR, Fiebach CJ. How the brain integrates costs and benefits during decision making. Proceedings of the National Academy of Sciences. 2010;107: 21767–21772. doi:10.1073/pnas.0908104107

35. Milosavljevic M, Malmaud J, Huth A, Koch C, Rangel A. The Drift Diffusion Model can account for the accuracy and reaction time of value-based choices under high and low time pressure. Judgm decis mak. 2010;5: 437–449. doi:10.1017/S1930297500001285

36. Cavanagh JF, Wiecki TV, Cohen MX, Figueroa CM, Samanta J, Sherman SJ, et al. Subthalamic nucleus stimulation reverses mediofrontal influence over decision threshold. Nat Neurosci. 2011;14: 1462–1467. doi:10.1038/nn.2925

37. Hunt LT, Kolling N, Soltani A, Woolrich MW, Rushworth MFS, Behrens TEJ. Mechanisms underlying cortical activity during value-guided choice. Nat Neurosci. 2012;15: 470–476. doi:10.1038/nn.3017

38. Krajbich I, Lu D, Camerer C, Rangel A. The Attentional Drift-Diffusion Model Extends to Simple Purchasing Decisions. Front Psychol. 2012;3. doi:10.3389/fpsyg.2012.00193

39. Witthoft N, Sha L, Winawer J, Kiani R. Sensory and decision-making processes underlying perceptual adaptation. Journal of Vision. 2018;18: 10. doi:10.1167/18.8.10

40. Collewijn H, Erkelens CJ, Steinman RM. Binocular co-ordination of human horizontal saccadic eye movements. The Journal of Physiology. 1988;404: 157–182. doi:10.1113/jphysiol.1988.sp017284

41. Leigh RJ, Zee DS. The Neurology of Eye Movements. Oxford University Press; 2015.

42. Palmer J, Huk AC, Shadlen MN. The effect of stimulus strength on the speed and accuracy of a perceptual decision. Journal of Vision. 2005;5: 1. doi:10.1167/5.5.1

43. Smucny J, Hanks TD, Lesh TA, O'Reilly RC, Carter CS. Altered Associations Between Motivated Performance and Frontostriatal Functional Connectivity During Reward Anticipation in Schizophrenia. Schizophrenia Bulletin. 2023;49: 717–725. doi:10.1093/schbul/sbac204

44. Smucny J, Hanks TD, Lesh TA, Carter CS. Altered Associations Between Task Performance and Dorsolateral Prefrontal Cortex Activation During Cognitive Control in Schizophrenia. Biological Psychiatry: Cognitive Neuroscience and Neuroimaging. 2023;8: 1050–1057. doi:10.1016/j.bpsc.2023.05.010

45. Bansal S, Bray LCJ, Schwartz BL, Joiner WM. Transsaccadic Perception Deficits in Schizophrenia Reflect the Improper Internal Monitoring of Eye Movement Rather Than Abnormal Sensory Processing. Biological Psychiatry: Cognitive Neuroscience and Neuroimaging. 2018;3: 168–177. doi:10.1016/j.bpsc.2017.06.004

46. Schütt HH, Harmeling S, Macke JH, Wichmann FA. Painfree and accurate Bayesian estimation of psychometric functions for (potentially) overdispersed data. Vision Research. 2016;122: 105–123. doi:10.1016/j.visres.2016.02.002

47. Joiner WM, Shelhamer M. Responses to Noisy Periodic Stimuli Reveal Properties of a Neural Predictor. Journal of Neurophysiology. 2006;96: 2121–2126. doi:10.1152/jn.00490.2006

48. Joiner WM, Lee J-E, Shelhamer M. Behavioral analysis of predictive saccade tracking as studied by countermanding. Exp Brain Res. 2007;181: 307–320. doi:10.1007/s00221-007-0933-0

49. Bates D, Maechler M, Bolker B, Walker S. Fitting Linear Mixed-Effects Models Using lme4. Journal of Statistical Software. 2015;67: 1–48.

50. Kuznetsova A, Brockhoff PB, Christensen RHB. lmerTest: Tests in Linear Mixed Effects Models. 2015. Available: https://cran.r-project.org/web/packages/lmerTest/index.html

51. Bansal S, Joiner WM. Transsaccadic visual perception of foveal compared to peripheral environmental changes. Journal of Vision. 2021;21: 12. doi:10.1167/jov.21.6.12

52. Sommer MA, Wurtz RH. What the Brain Stem Tells the Frontal Cortex. II. Role of the SC-MD-FEF Pathway in Corollary Discharge. Journal of Neurophysiology. 2004;91: 1403–1423. doi:10.1152/jn.00740.2003

53. Crapse TB, Sommer MA. Corollary discharge circuits in the primate brain. Current Opinion in Neurobiology. 2008;18: 552–557. doi:10.1016/j.conb.2008.09.017

54. Hamker FH, Zirnsak M, Calow D, Lappe M. The Peri-Saccadic Perception of Objects and Space. Friston KJ, editor. PLoS Comput Biol. 2008;4: e31. doi:10.1371/journal.pcbi.0040031

55. Keith GP, Crawford JD. Saccade-related remapping of target representations between topographic maps: a neural network study. J Comput Neurosci. 2008;24: 157–178. doi:10.1007/s10827-007-0046-6

56. Masselink J, Lappe M. Visuomotor learning from postdictive motor error. eLife. 2021;10: e64278. doi:10.7554/eLife.64278

57. Butler PD, Schechter I, Zemon V, Schwartz SG, Greenstein VC, Gordon J, et al. Dysfunction of Early-Stage Visual Processing in Schizophrenia. AJP. 2001;158: 1126–1133. doi:10.1176/appi.ajp.158.7.1126

58. Martínez A, Hillyard SA, Dias EC, Hagler DJ, Butler PD, Guilfoyle DN, et al. Magnocellular Pathway Impairment in Schizophrenia: Evidence from Functional Magnetic Resonance Imaging. J Neurosci. 2008;28: 7492–7500. doi:10.1523/JNEUROSCI.1852-08.2008

59. Adámek P, Langová V, Horáček J. Early-stage visual perception impairment in schizophrenia, bottom-up and back again. Schizophr. 2022;8: 27. doi:10.1038/s41537-022-00237-9

60. Adámek P, Grygarová D, Jajcay L, Bakštein E, Fürstová P, Juríčková V, et al. The Gaze of Schizophrenia Patients Captured by Bottom-up Saliency. Schizophr. 2024;10: 21. doi:10.1038/s41537-024-00438-4

61. Shadlen MN, Newsome WT. Motion perception: seeing and deciding. Proceedings of the National Academy of Sciences. 1996;93: 628–633. doi:10.1073/pnas.93.2.628

62. Roitman JD, Shadlen MN. Response of Neurons in the Lateral Intraparietal Area during a Combined Visual Discrimination Reaction Time Task. J Neurosci. 2002;22: 9475–9489. doi:10.1523/JNEUROSCI.22-21-09475.2002

63. Brody CD, Hanks TD. Neural underpinnings of the evidence accumulator. Current Opinion in Neurobiology. 2016;37: 149–157. doi:10.1016/j.conb.2016.01.003

64. Shadlen MN, Newsome WT. Neural Basis of a Perceptual Decision in the Parietal Cortex (Area LIP) of the Rhesus Monkey. Journal of Neurophysiology. 2001;86: 1916–1936. doi:10.1152/jn.2001.86.4.1916

65. Sommer MA, Wurtz RH. Influence of the thalamus on spatial visual processing in frontal cortex. Nature. 2006;444: 374–377. doi:10.1038/nature05279

66. Sommer MA, Wurtz RH. A Pathway in Primate Brain for Internal Monitoring of Movements. Science. 2002;296: 1480–1482. doi:10.1126/science.1069590

67. Cavanaugh J, Berman RA, Joiner WM, Wurtz RH. Saccadic Corollary Discharge Underlies Stable Visual Perception. J Neurosci. 2016;36: 31–42. doi:10.1523/JNEUROSCI.2054-15.2016

68. Hikosaka O, Takikawa Y, Kawagoe R. Role of the Basal Ganglia in the Control of Purposive Saccadic Eye Movements. Physiological Reviews. 2000;80: 953–978. doi:10.1152/physrev.2000.80.3.953

69. Scudder CA, Kaneko CR, Fuchs AF. The brainstem burst generator for saccadic eye movements. Exp Brain Res. 2002;142: 439–462. doi:10.1007/s00221-001-0912-9

70. Quinet J, Goffart L. Cerebellar control of saccade dynamics: contribution of the fastigial oculomotor region. Journal of Neurophysiology. 2015;113: 3323–3336. doi:10.1152/jn.01021.2014

71. Moberget T, Ivry RB. Prediction, Psychosis, and the Cerebellum. Biological Psychiatry: Cognitive Neuroscience and Neuroimaging. 2019;4: 820–831. doi:10.1016/j.bpsc.2019.06.001

72. Collins AGE, Brown JK, Gold JM, Waltz JA, Frank MJ. Working Memory Contributions to Reinforcement Learning Impairments in Schizophrenia. J Neurosci. 2014;34: 13747–13756. doi:10.1523/JNEUROSCI.0989-14.2014

Supporting Information Captions

Fig S1. Flowchart depicting the steps from the encoding of the visual error to the computation of the drift rate offset in the drift diffusion modeling framework.

Participants completed the trans-saccadic task by pressing one of two buttons representing either perceptual judgment. The visual error encoded the difference from the eye endpoint location to the shifted visual target. Visual error predicted button response accuracy and the corresponding VE predictive weights were extracted. Such weights were the basis for the drift rate offset in the DDM framework. See Materials and Methods for full description of each step of the framework.

Fig S2. VE-based logistic psychometric functions at group level and at the level of the individual depicted on Fig 8.

Psychometric curves (continuous purple line) fitted to the percentage of hypothetical forward response data (individual filled circles) that correspond to the case in which participants would have solely relied on the VE. Fits were computed based on a logistic function. A dashed line indicates the theoretical shift from backward to forward VEs with a step function. (A) Group-level psychometric data across 4° and 8° saccade jumps and averaged. Individual filled circles correspond to group % forward response means for each target shift, along with their SEM, as shown with error bars. The logistic function is fit with a fixed [0,1] range. (B) Individual psychometric data for an example subject. Individual filled circles correspond to the subject % forward response means at each target shift.

Fig S3. Group VE-based psychometric function separated by saccade amplitude and direction of saccade.

Psychometric functions (black continuous line) fitted to the percentage of hypothetical forward response data (individual filled circles) that correspond to the case in which participants would have solely relied on the VE. Fits were computed at the group level based on the *psignifit* method (psychometric function) as detailed in the manuscript to describe the results from Fig 6. Psychometric results are broken down into 4° and 8° trials (left and right columns respectively), and into leftward, rightward, and all saccade types (rows 1, 2, and 3 respectively).

Fig S4. Individual VE-based psychometric function separated by saccade amplitude and direction of saccade

Psychometric functions (black continuous line) fitted to the percentage of hypothetical forward response data (individual filled circles) that correspond to the case in which participants would have solely relied on the VE. Fits were computed for the individual corresponding to the data on Fig 8 based on the *psignifit* method (psychometric function), as detailed in the manuscript to describe the results from Fig 6. Psychometric results are broken down into 4° and 8° trials (left and right columns respectively), and into leftward, rightward, and all saccade types (rows 1, 2, and 3 respectively).

S1 Appendix. Additional information pertaining to the DDM.

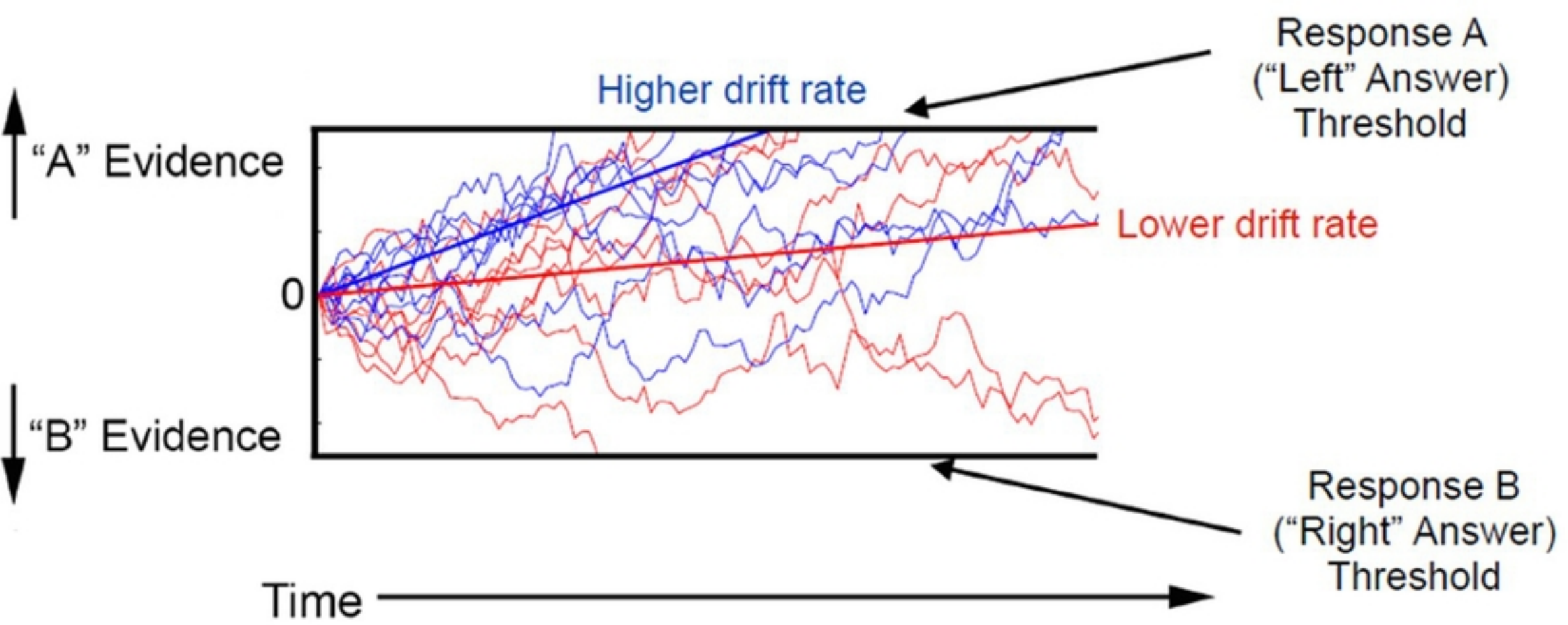
Response A
("Left" Answer)
Threshold
Higher drift rate
"A" Evidence
Lower drift rate
0
"B" Evidence
Response B
("Right" Answer)
Threshold
Time

Fig3

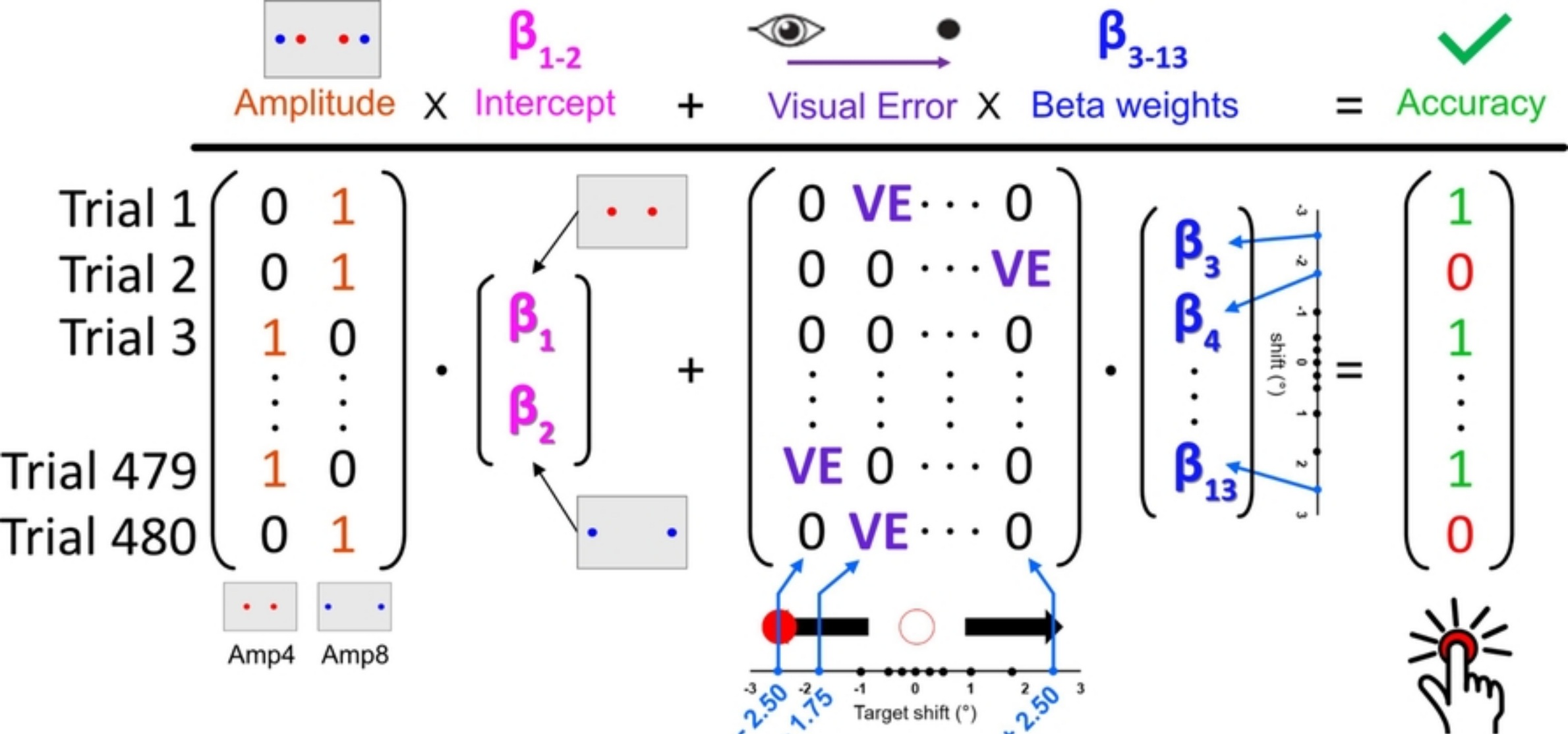
Amplitude
X
β1-2
Intercept
+
Visual Error
X
β3-13
Beta weights
=
Accuracy
Trial 1
Trial 2
Trial 3
Trial 479
Trial 480
0 1
0 1
1 0
1 0
0 1
Amp4
Amp8
β1
β2
0 VE · · · 0
0 0 · · · VE
0 0 · · · 0
VE 0 · · · 0
0 VE · · · 0
-2.50
-1.75
Target shift (°)
+2.50
β3
β4
β13
shift (°)
1
0
1
1
0

Fig2

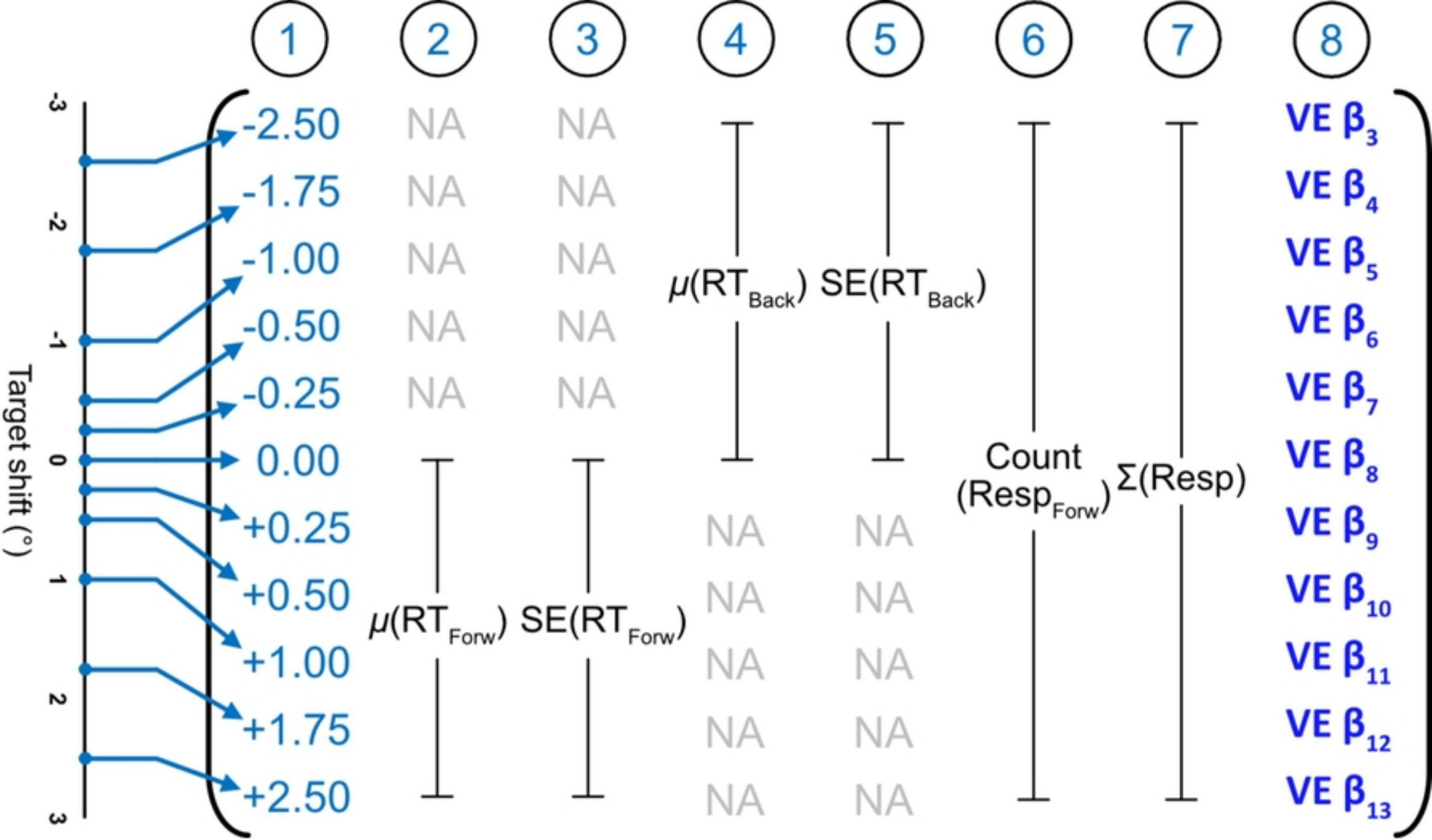
1
2
3
4
5
6
7
8
Target shift (°)
-3
-2
-1
0
1
2
3
-2.50
-1.75
-1.00
-0.50
-0.25
0.00
+0.25
+0.50
+1.00
+1.75
+2.50
NA
μ(RT_Forw)
SE(RT_Forw)
μ(RT_Back)
SE(RT_Back)
Count (Resp_Forw)
Σ(Resp)
VE β3
VE β4
VE β5
VE β6
VE β7
VE β8
VE β9
VE β10
VE β11
VE β12
VE β13

Fig4

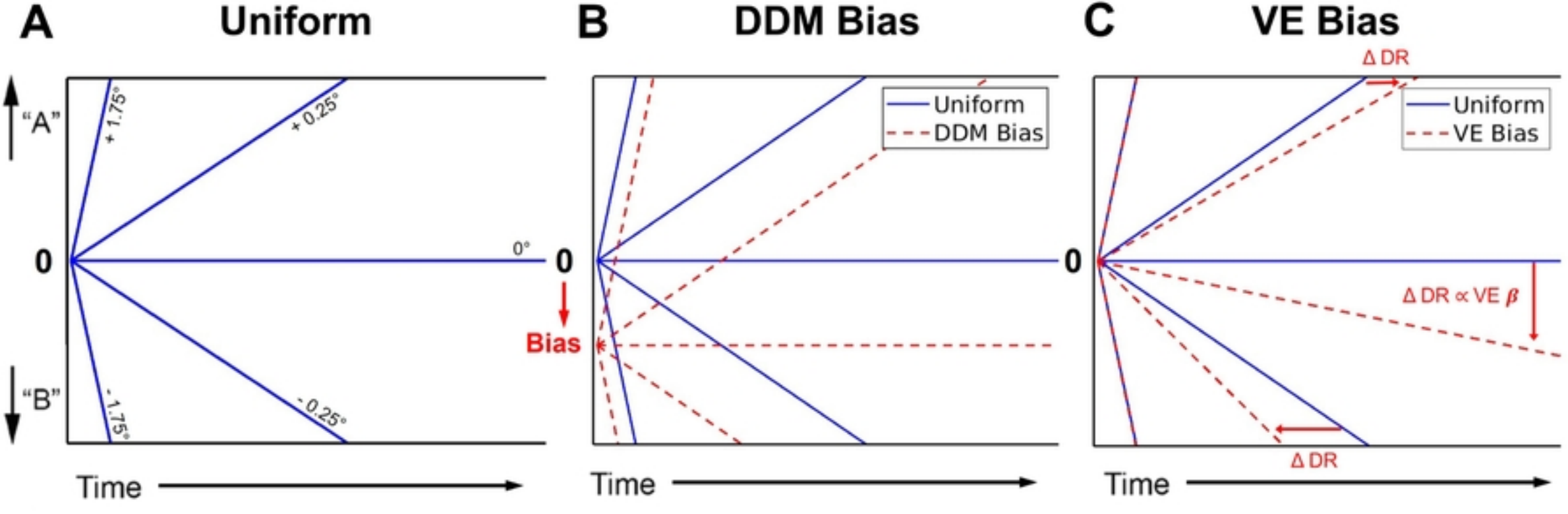
A
Uniform
"A"
"B"
+ 1.75°
+ 0.25°
0°
- 0.25°
- 1.75°
0
Time
B
DDM Bias
Uniform
DDM Bias
0
Bias
Time
C
VE Bias
Δ DR
Uniform
VE Bias
0
Δ DR ∝ VE β
Δ DR
Time

Fig5

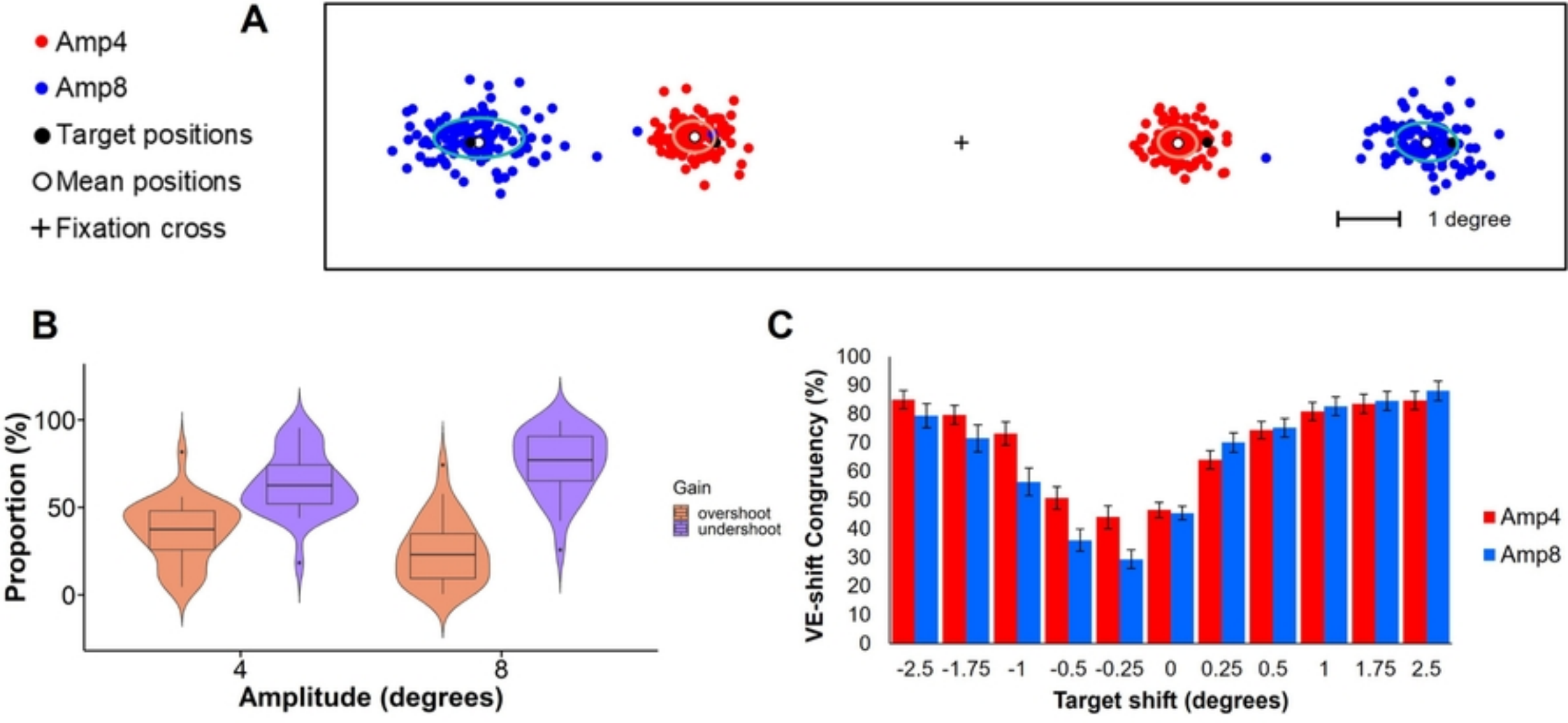
A
Amp4
Amp8
Target positions
Mean positions
Fixation cross
1 degree
B
Proportion (%)
100
50
0
4
8
Amplitude (degrees)
Gain
overshoot
undershoot
C
VE-shift Congruency (%)
100
90
80
70
60
50
40
30
20
10
0
-2.5 -1.75 -1 -0.5 -0.25 0 0.25 0.5 1 1.75 2.5
Target shift (degrees)
Amp4
Amp8

Fig7

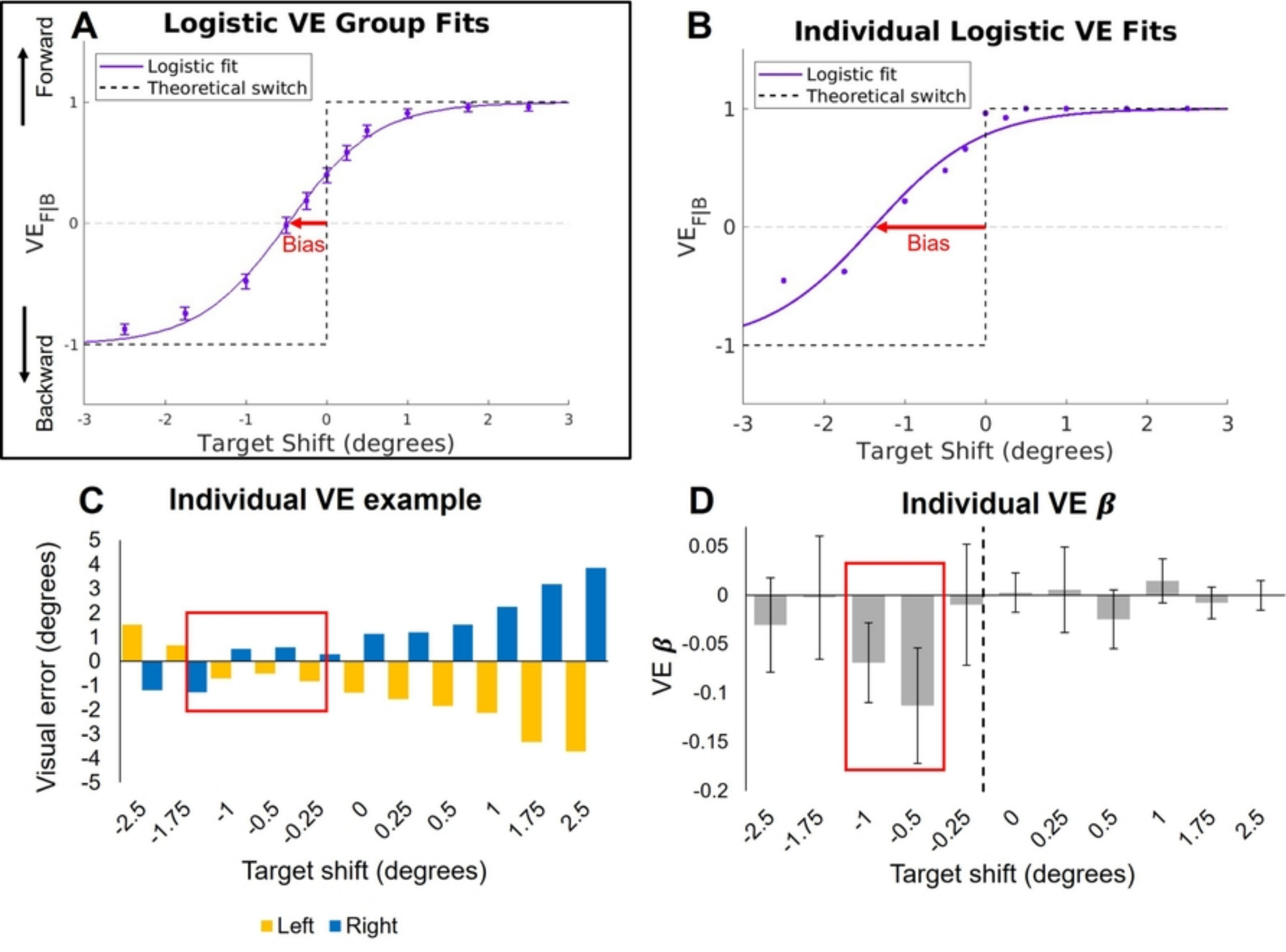
A
Logistic VE Group Fits
Forward
Backward
Logistic fit
Theoretical switch
Bias
$VE_{F|B}$
Target Shift (degrees)
B
Individual Logistic VE Fits
Logistic fit
Theoretical switch
Bias
$VE_{F|B}$
Target Shift (degrees)
C
Individual VE example
Visual error (degrees)
Target shift (degrees)
Left
Right
D
Individual VE β
VE β
Target shift (degrees)

Fig8

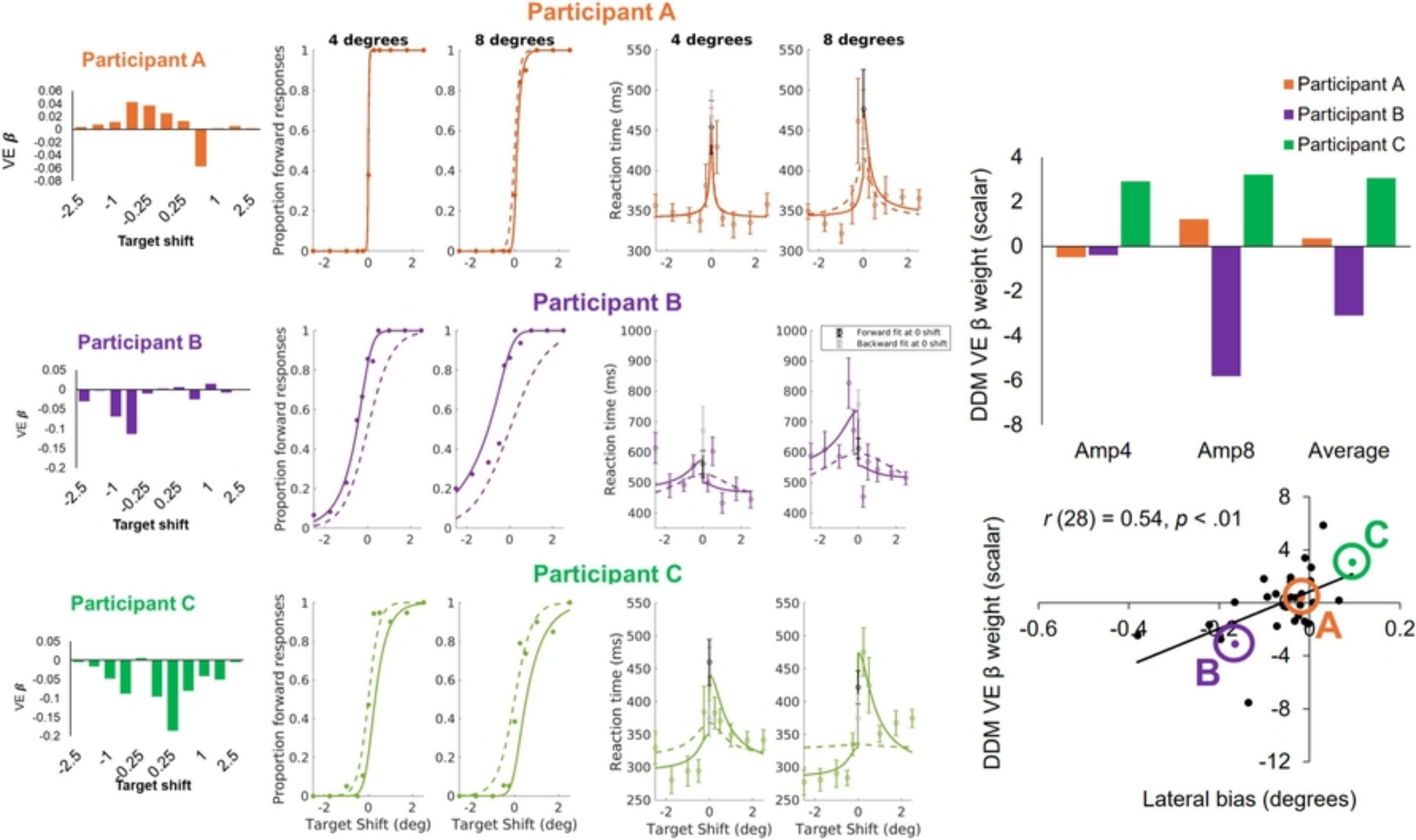
Participant A
4 degrees
8 degrees
4 degrees
8 degrees
Participant A
VE β
Target shift
Proportion forward responses
Reaction time (ms)
Participant B
Participant B
VE β
Target shift
Proportion forward responses
Reaction time (ms)
Forward fit at 0 shift
Backward fit at 0 shift
Participant C
Participant C
VE β
Target shift
Proportion forward responses
Reaction time (ms)
Target Shift (deg)
Target Shift (deg)
Target Shift (deg)
Target Shift (deg)
Participant A
Participant B
Participant C
DDM VE β weight (scalar)
Amp4
Amp8
Average
r (28) = 0.54, p < .01
DDM VE β weight (scalar)
Lateral bias (degrees)
A
B
C

Fig10

A Task Procedure

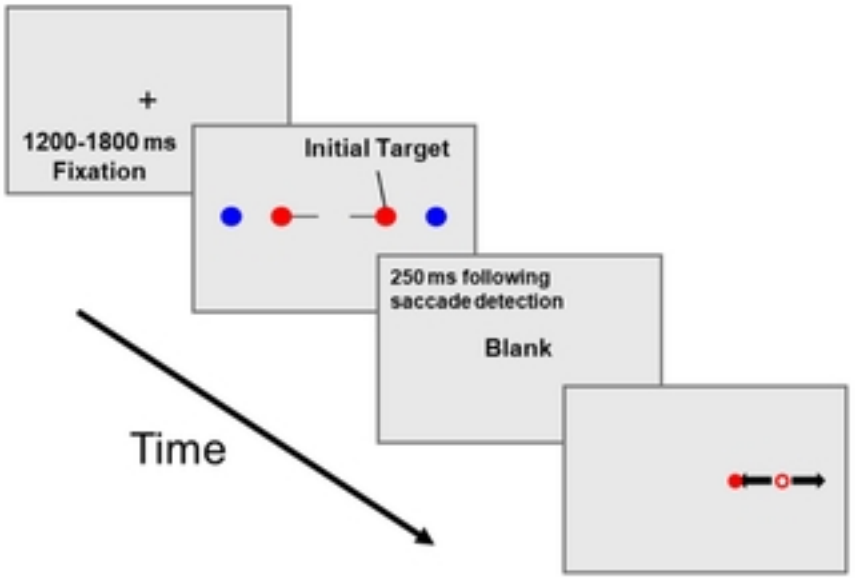

B Estimation of Psychometric Threshold and Bias

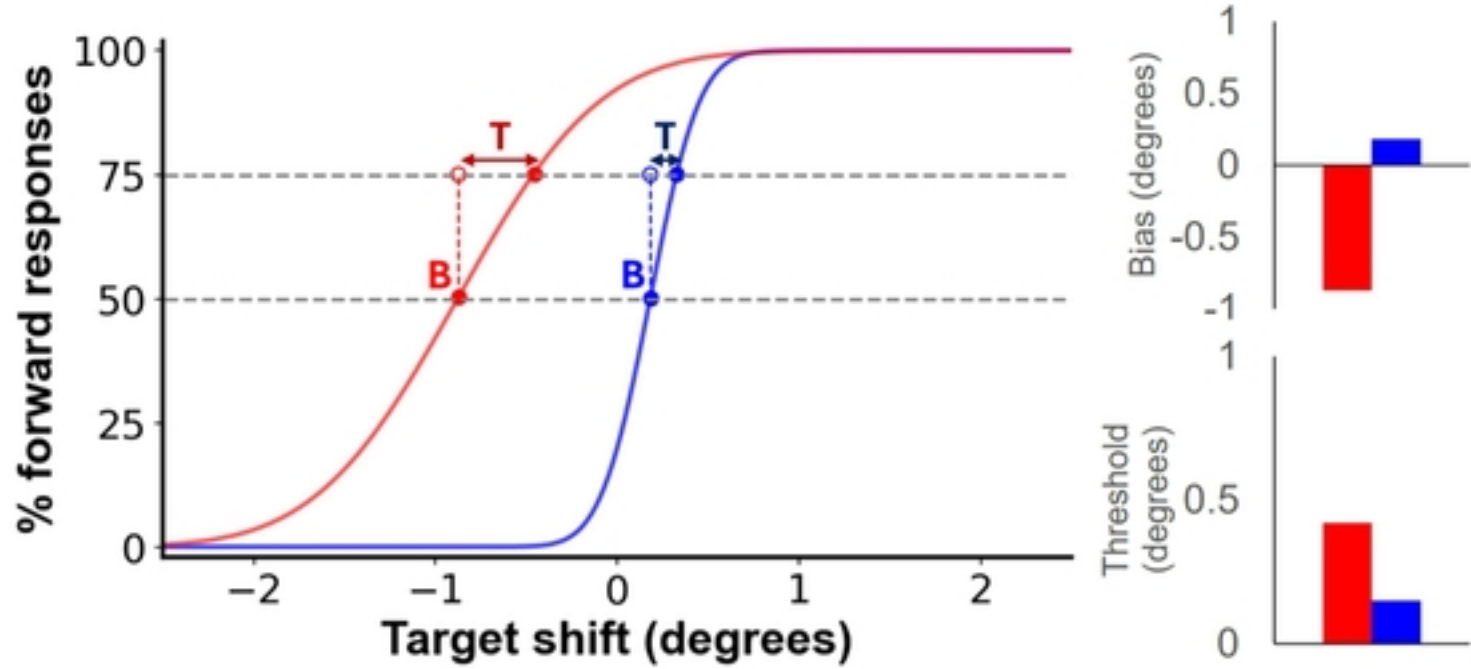

C Estimation of Visual Error

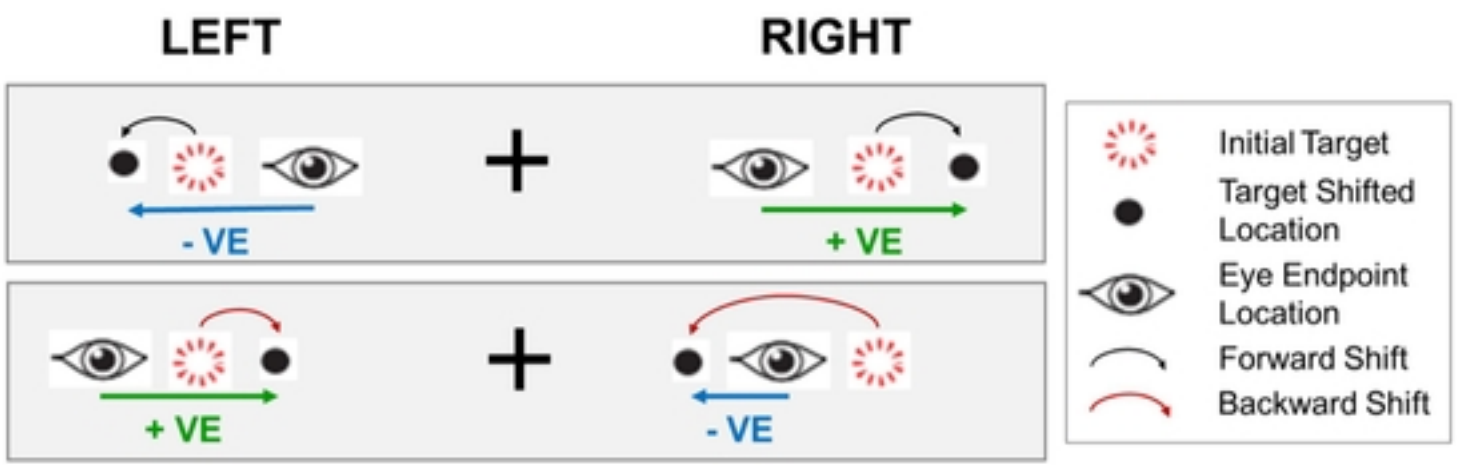

Fig1

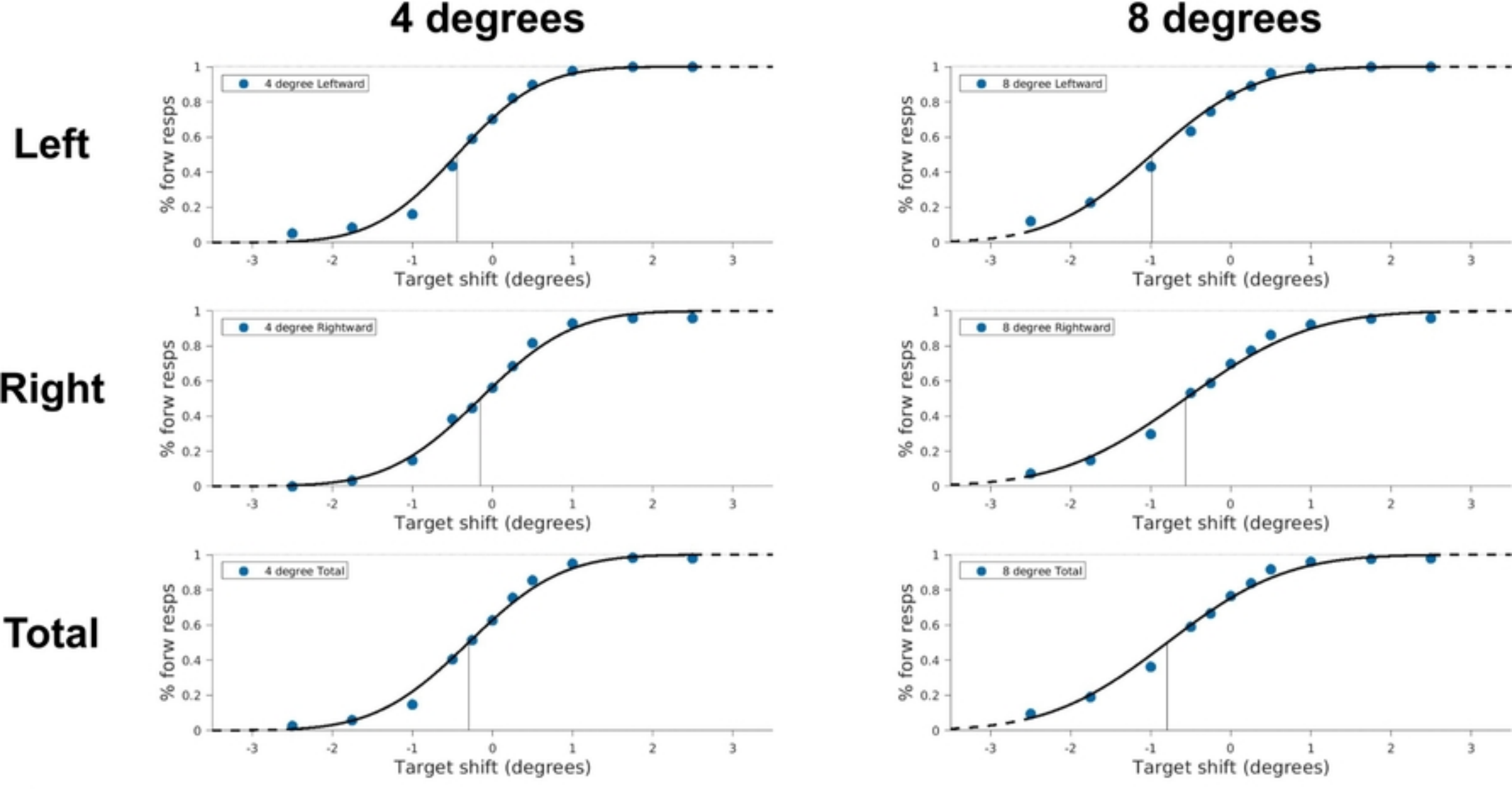
4 degrees
8 degrees
Left
Right
Total
4 degree Leftward
8 degree Leftward
4 degree Rightward
8 degree Rightward
4 degree Total
8 degree Total
% forw resps
Target shift (degrees)

FigS3

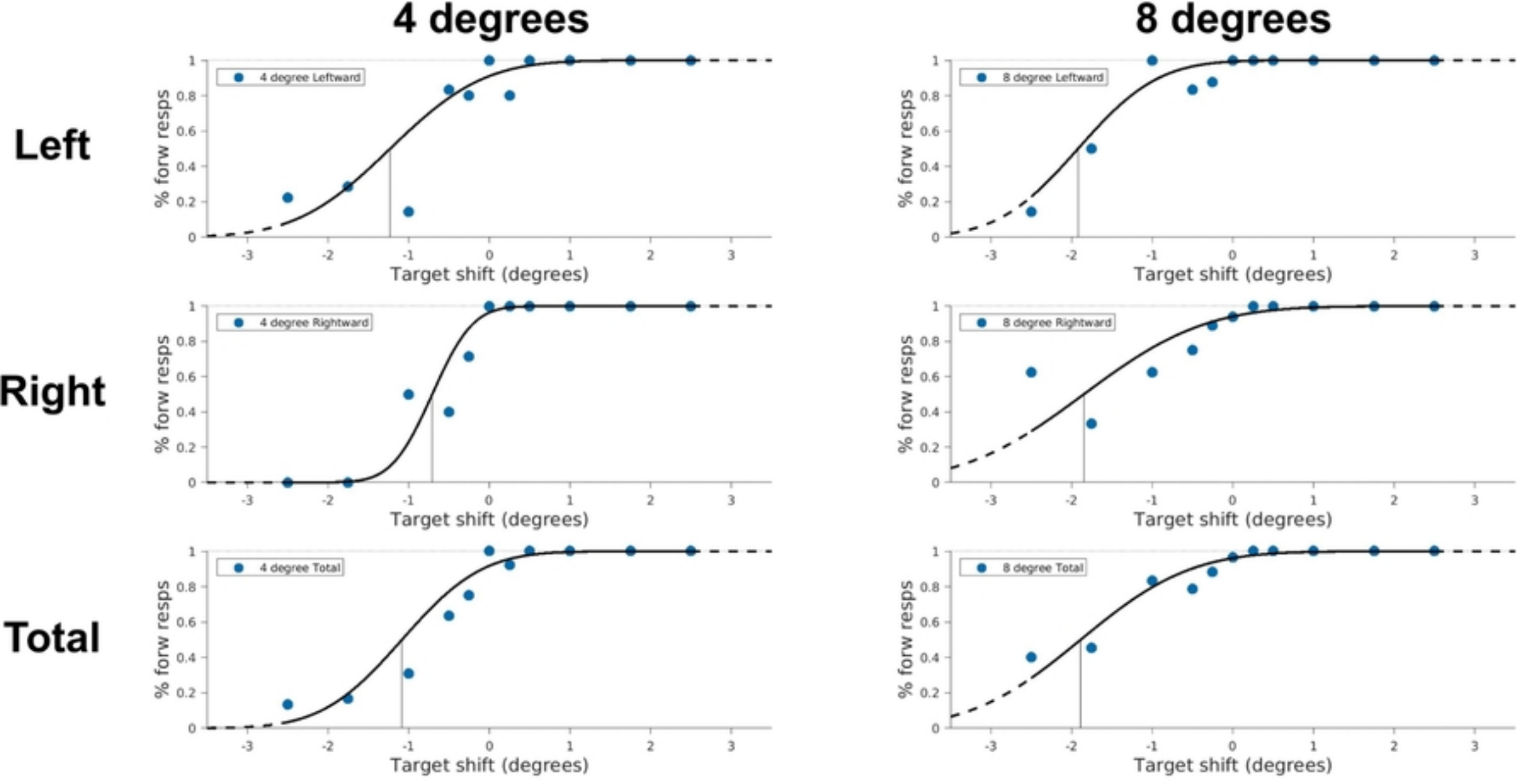
4 degrees
8 degrees
Left
Right
Total
4 degree Leftward
8 degree Leftward
4 degree Rightward
8 degree Rightward
4 degree Total
8 degree Total
% forw resps
Target shift (degrees)

FigS4

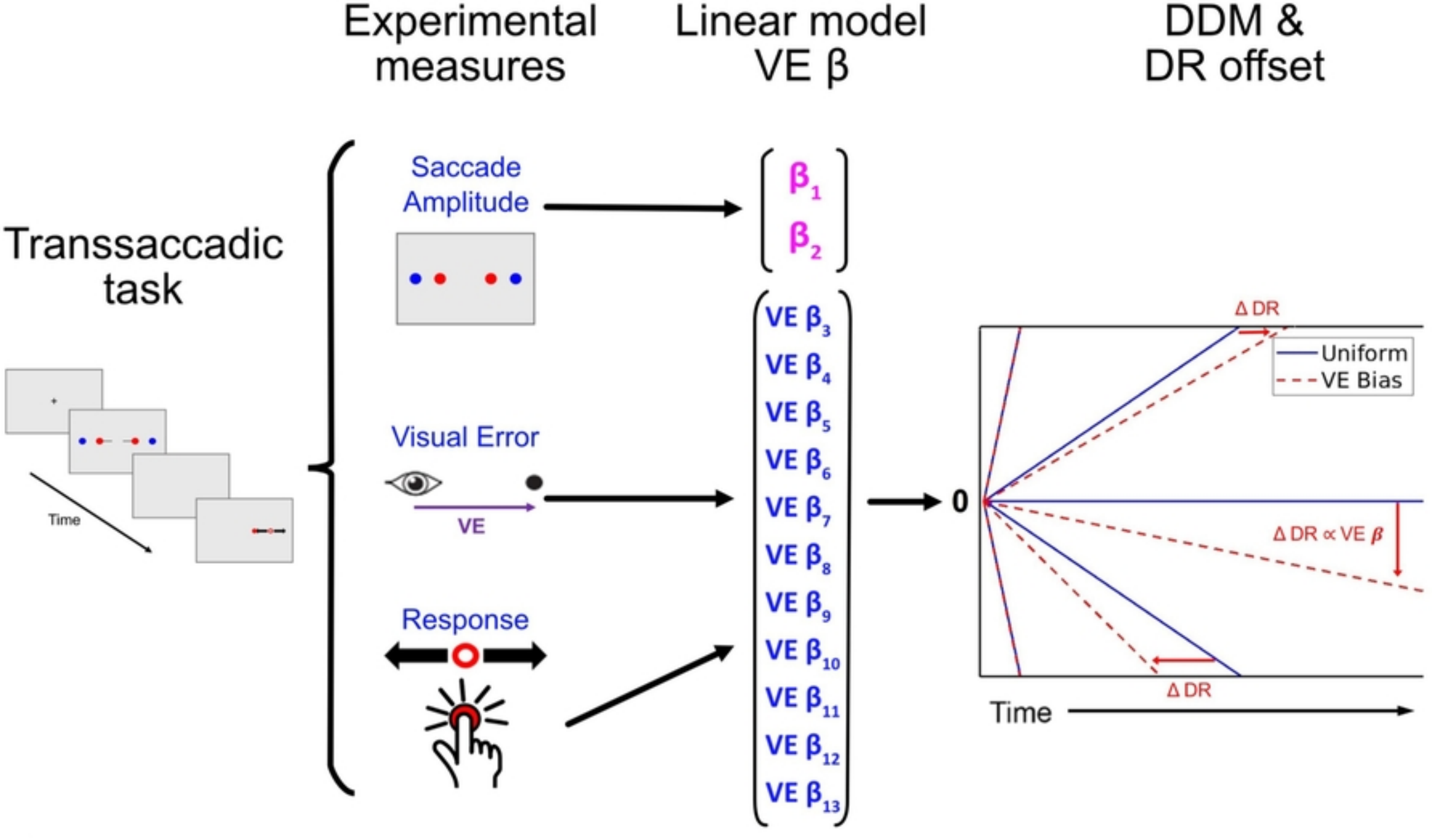
Experimental measures
Linear model VE β
DDM & DR offset
Transsaccadic task
Time
Saccade Amplitude
Visual Error
VE
Response
β1
β2
VE β3
VE β4
VE β5
VE β6
VE β7
VE β8
VE β9
VE β10
VE β11
VE β12
VE β13
0
Δ DR
Uniform
VE Bias
Δ DR ∝ VE β
Δ DR
Time

FigS1

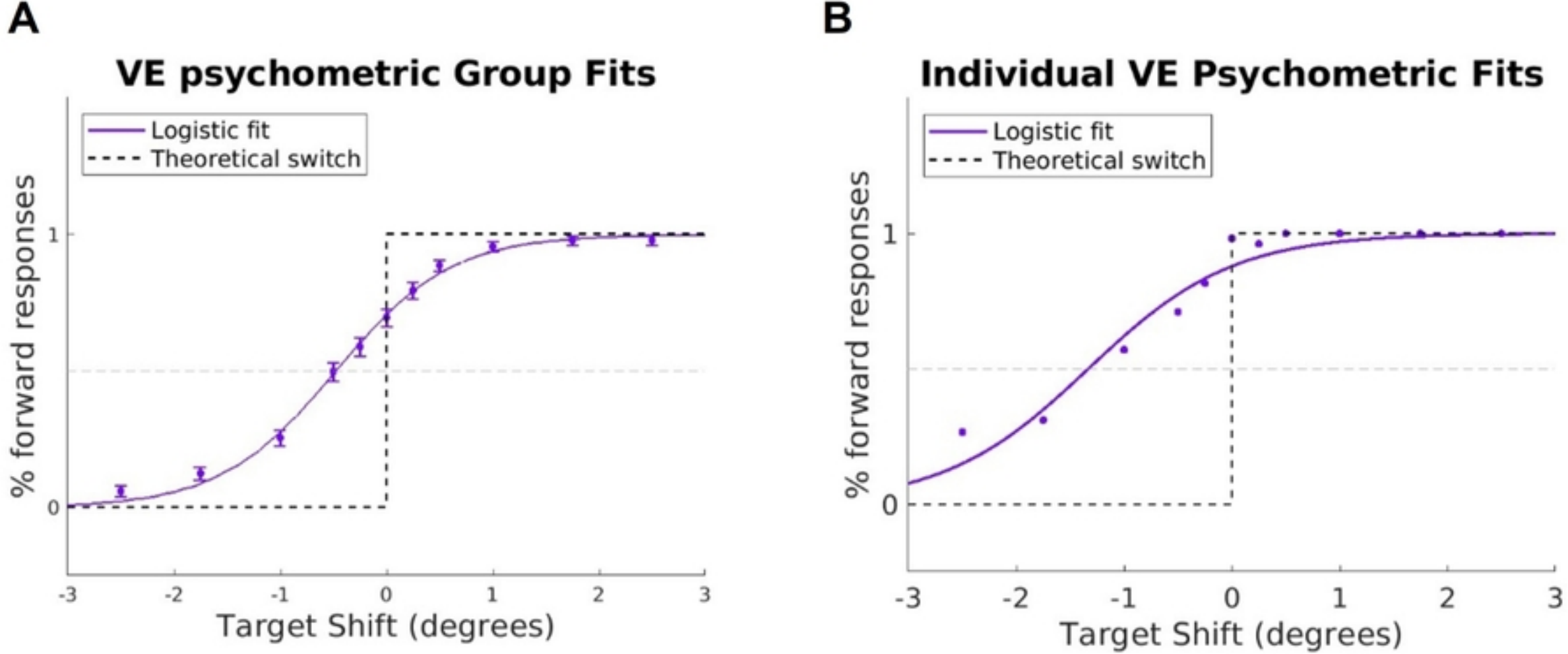
A
VE psychometric Group Fits
Logistic fit
Theoretical switch
% forward responses
1
0
-3
-2
-1
0
1
2
3
Target Shift (degrees)
B
Individual VE Psychometric Fits
Logistic fit
Theoretical switch
% forward responses
1
0
-3
-2
-1
0
1
2
3
Target Shift (degrees)

FigS2

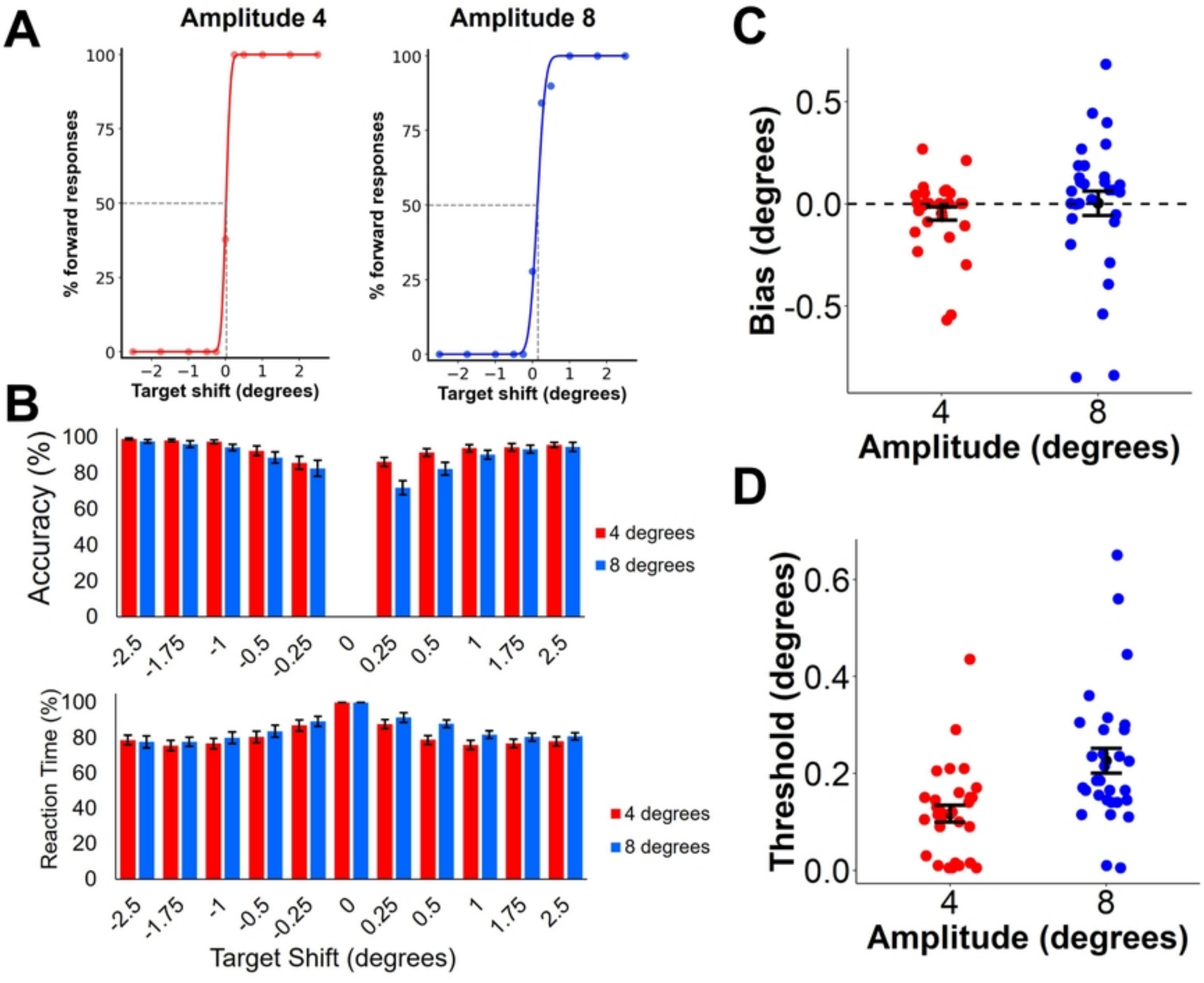
A
Amplitude 4
Amplitude 8
% forward responses
Target shift (degrees)
B
Accuracy (%)
Reaction Time (%)
4 degrees
8 degrees
Target Shift (degrees)
C
Bias (degrees)
Amplitude (degrees)
D
Threshold (degrees)
Amplitude (degrees)

Fig6

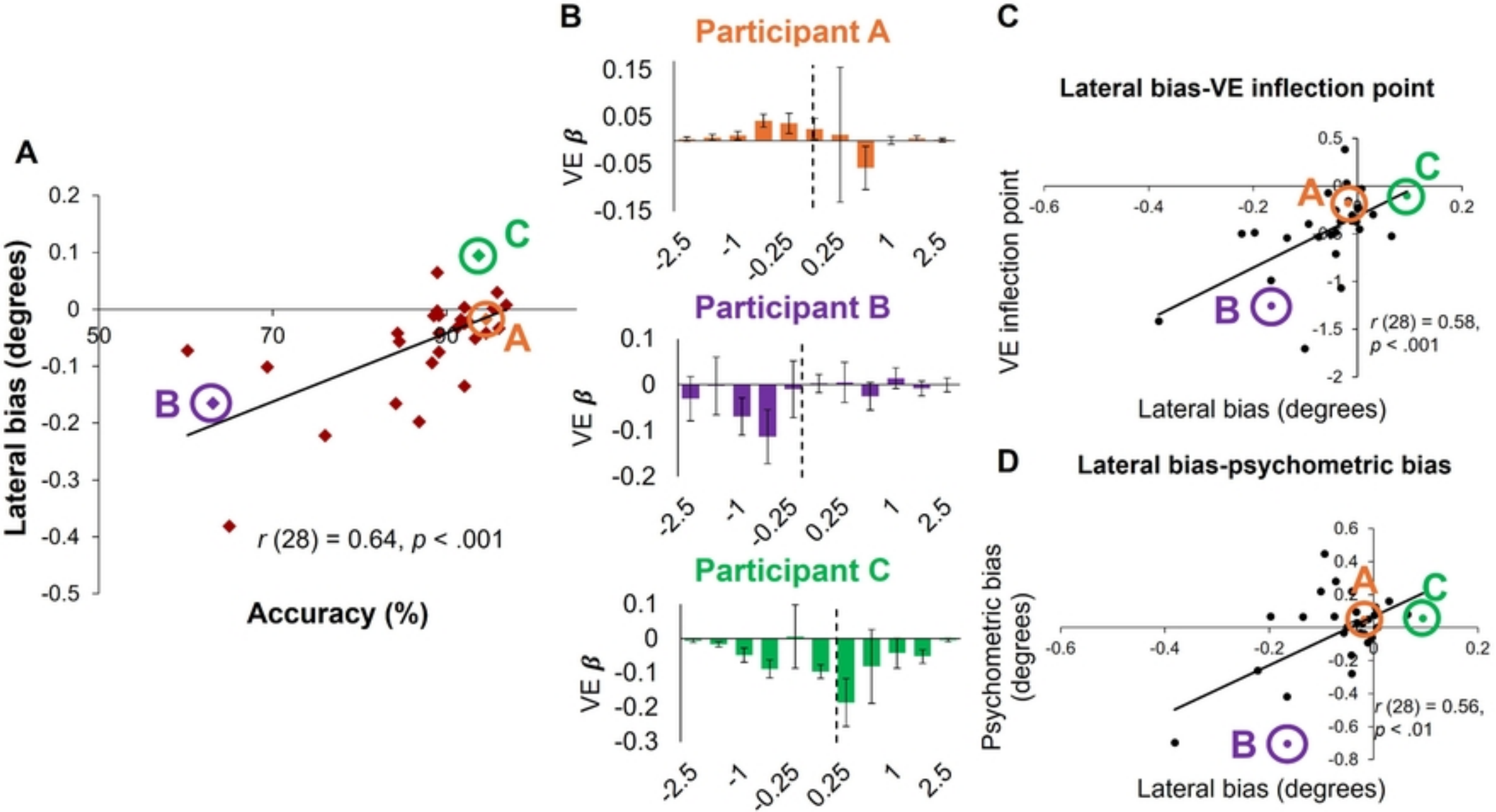
A
Lateral bias (degrees)
Accuracy (%)
r (28) = 0.64, p < .001
B
Participant A
Participant B
Participant C
VE β
C
Lateral bias-VE inflection point
VE inflection point
Lateral bias (degrees)
r (28) = 0.58, p < .001
D
Lateral bias-psychometric bias
Psychometric bias (degrees)
Lateral bias (degrees)
r (28) = 0.56, p < .01

Fig9